Article

Differential Roles of the Calcium Ion Channel TRPV4 in Host Responses to *Mycobacterium tuberculosis* Early and Late in Infection

Sumanta Kumar Naik, Kaliprasad Pattanaik, Jacqueline Eich, ..., Wolfgang M. Kuebler, Ulrich E. Schaible, Avinash Sonawane

uschaible@fz-borstel.de (U.E.S.)
asonawane@iiti.ac.in (A.S.)

HIGHLIGHTS

Mtb down-modulates TRPV4 expression in macrophages

Trpv4−/− macrophages cannot be activated to drive phagosome maturation and NO production

Trpv4-deficient mice are more resistant to Mtb

TRPV4-positive macrophages in the periphery of human granuloma but not at the center

iScience

Article

Differential Roles of the Calcium Ion Channel TRPV4 in Host Responses to *Mycobacterium tuberculosis* Early and Late in Infection

Sumanta Kumar Naik,[1,2] Kaliprasad Pattanaik,[1] Jacqueline Eich,[2] Vivien Sparr,[2] Matthias Hauptmann,[2] Barbara Kalsdorf,[2] Norbert Reiling,[2] Wolfgang Liedtke,[3] Wolfgang M. Kuebler,[4] Ulrich E. Schaible,[2,6,7,*] and Avinash Sonawane[1,5,6,*]

SUMMARY

***Mycobacterium tuberculosis* subverts host immunity to proliferate within host tissues. Non-selective transient receptor potential (TRP) ion channels are involved in host responses and altered upon bacterial infections. Altered expression and localization of TRPV4 in macrophages upon virulent *M. tuberculosis* infection together with differential distribution of TRPV4 in human tuberculosis (TB) granulomas indicate a role of TRPV4 in TB. Compared with wild-type mice, Trpv4-deficient littermates showed transiently higher mycobacterial burden and reduced proinflammatory responses. In the absence of TRPV4, activation failed to render macrophages capable of controlling mycobacteria. Surprisingly, Trpv4-deficient mice were superior to wild-type ones in controlling *M. tuberculosis* infection in the chronic phase. Thus, Trpv4 is important in host responses to mycobacteria, although with opposite functions early versus late in infection. Ameliorated chronic infection in the absence of Trpv4 and its expression in human TB lesions indicate TRPV4 as putative target for host-directed therapy.**

INTRODUCTION

Emerging data indicate a role for calcium ion channels in bacterial infections (Deretic and Fratti, 1999; King et al., 2020). Bacterial endotoxin can activate transient receptor potential (TRP) channels including TRPV4 in airway epithelial cells, which triggers proinflammatory responses (Alpizar et al., 2017). The host endeavors to eliminate a pathogen, whereas the pathogen strives to control or escape host defenses. Macrophages are in principle equipped to eliminate bacterial pathogens, but are exploited by virulent *Mycobacterium tuberculosis* as their primary resident host cells by circumventing the macrophage's host defense armamentarium. *M. tuberculosis*, the causative agent of human tuberculosis (TB), successfully escapes host defense to establish infection by modulating intracellular trafficking and intracellular calcium signaling as well as through induction of necrotic cell death. However, exposure of macrophages to extracellular ATP and interferon-gamma (IFN-γ) promotes phagosome acidification, generation of reactive nitrogen species (RNS), and apoptosis over necrotic cell death, and hence intracellular killing of *M. tuberculosis*. Mutants lacking the region of differentiation-1 (RD1) encompassing the *esx1*-encoded type 7 secretion system, beside others, are attenuated by failing both, inhibition of phagosome maturation and induction of necrotic cell death. The Esx1-associated small secreted proteins, early secretory antigen target-6 (ESAT-6) and culture filtrate protein 10 (CFP10), are involved in inhibition of phagosome acidification (de Jonge et al., 2007).

Among the protein family of calcium ion channels, TRP ion channels are involved in immune responses within the lung microenvironment (Venkatachalam and Montell, 2007). TRPA1 is expressed in foamy macrophages and regulates cholesterol metabolism and anti-inflammatory response. TRPM8 and TRPV1 are expressed in lung epithelial cells and are crucial for the synthesis of proinflammatory cytokines, e.g., interleukin (IL)-6, IL-8, tumor necrosis factor (TNF)-α, IL-1α, and IL-1β (Sabnis et al., 2008; Reilly et al., 2005). TRPV4 is highly expressed in alveolar epithelial cells, endothelial cells, neutrophils, and macrophages and important for pro-inflammatory responses, goblet cell recruitment, and airway wall thickening during inflammatory lung diseases (Jia et al., 2004; Moran et al., 2011; Suresh et al., 2015; Gombedza et al., 2017).

[1]School of Biotechnology, KIIT University, Odisha 751024, India

[2]Program Area Infections, Department of Cellular Microbiology, Research Center Borstel-Leibniz Lung Center, Borstel 23845, Germany

[3]Duke University Center for Translational Neuroscience, Durham, NC 27710, USA

[4]Institute of Physiology, Charité–Universitäts-medizin, Berlin, Germany

[5]Discipline of Biosciences & Biomedical Engineering, Indian Institute of Technology, Indore, Madhya Pradesh 453552, India

[6]These authors contributed equally

[7]Lead Contact

*Correspondence: uschaible@fz-borstel.de (U.E.S.), asonawane@iiti.ac.in (A.S.) https://doi.org/10.1016/j.isci.2020.101206

Consequently, pharmacological inhibitors of TRPV4 have been considered as therapeutics of acute lung injury (Balakrishna et al., 2014). Inhibition of TRPV4 is associated with impaired *in vitro* neutrophil responses including chemotaxis (Yin et al., 2016). *M. tuberculosis* is known to inhibit calcium signaling in macrophages to reduce phago-lysosome fusion and secure intracellular survival (Malik et al., 2000). These studies strongly suggest that calcium regulation by TRPV4 may be crucially involved in inflammatory lung diseases. To date, there is no report on the role of TRPV4 in *M. tuberculosis* infection. We found that wild-type (WT) *M. tuberculosis,* but not an attenuated ΔRD1 mutant, can down-regulate *Trpv4* expression, thereby inhibiting intracellular calcium mobilization. IFN-γ-activated *Trpv4*$^{-/-}$ macrophages failed to restrict *M. tuberculosis* growth due to limited phagosome maturation and nitrite (NO$_2^-$) production. *Trpv4*$^{-/-}$ mice showed higher *M. tuberculosis* lung burden associated with lower proinflammatory responses at early time points of infection. However, in the chronic phase of infection, *Trpv4*-deficient mice were superior to WT mice in controlling mycobacterial growth. Our data indicate that *M. tuberculosis* alters TRPV4 expression to facilitate the infection progress. At the late phase of infection, though, TRPV4 facilitates mycobacterial growth indicating TRPV4 as a host-directed therapeutic target for subsidiary treatment of antibiotic therapy of TB.

RESULTS

Trpv4 Expression in Macrophages Is Altered by *M. tuberculosis*

To understand Trpv4 regulation during *M. tuberculosis* infection, we analyzed TRPV4 in *M. tuberculosis*-H37Rv-infected murine bone marrow-derived macrophages (BMDM) at protein level. Confocal microscopy revealed association of TRPV4 with the macrophage plasma membrane at 2 h (Figure 1A, upper panel) but dispersed localization at 24 h post-infection (p.i.) (Figure 1A, lower panel). Quantification of TRPV4 protein expression in infected BMDM lysates by western blot showed *M. tuberculosis*-H37Rv induced TRPV4 down-regulation at both 24 and 48 h p.i. (Figure 1B). In contrast, infection with *M. tuberculosis* ΔRD1 transiently down-regulated TRPV4 expression at 24 h but not 48 h p.i. Analysis of *Trpv4* mRNA expression by qRT-PCR in human monocyte-derived macrophages revealed a multiplicity of infection (MOI)-dependent increase in transcript numbers between MOI 1 and 3, which became, however, reduced again at MOI 10 (Figure 1C). These results demonstrate that infection of macrophages with virulent *M. tuberculosis*-H37Rv redistributes TRPV4 and regulates its expression in an MOI-dependent manner and that loss of TRPV4 is probably not due to reduced, but rather partially compensated, by higher transcription rates.

M. tuberculosis Survives in Activated Macrophages in the Absence of *Trpv4*

To assess the role of *Trpv4* in intracellular survival and growth of *M. tuberculosis*, we compared mycobacterial burden in WT and *Trpv4*$^{-/-}$ BMDM, alveolar, as well as peritoneal, macrophages, which were either left at the resting state or were stimulated with IFN-γ (Figures 1D–1F). Compared with WT cells, we observed a slightly better growth of *M. tuberculosis*-H37Rv in resting *Trpv4*-deficient BMDM and alveolar, but not peritoneal, macrophages. However, IFN-γ-activated *Trpv4*$^{-/-}$ macrophages of all three types were significantly less capable to restrict the growth of *M. tuberculosis* counts at 48 and 72 h p.i. when compared with WT cells (Figures 1D–1F). Notably, resting WT but not *Trpv4*$^{-/-}$ BMDM were able to control intracellular growth of the *M. tuberculosis* ΔRD1 mutant 48 and 72 h p.i. (Figure 1G). Similarly, *Mycobacterium smegmatis*, otherwise controlled by WT BMDM were able to grow in *Trpv4*$^{-/-}$ cells (Figure S1A). These data were further corroborated by experiments wherein we pretreated the RAW264.7 macrophage cell line with the pharmacological TRPV4 inhibitor RN1734 (10 μM) followed by *M. tuberculosis* infection. Higher *M. tuberculosis* counts were found in RN1734-treated RAW cells when compared with mock-treated controls at 48 h p.i. (Figure S1B). To control for differential phagocytosis rates between resting and IFN-γ-activated WT and *Trpv4*$^{-/-}$ macrophages, which may influence subsequent growth, we counted *M. tuberculosis* numbers at 2 h p.i., which, however, were comparable between resting and activated WT and *Trpv4*$^{-/-}$ BMDMs (Figure S1C). Taken together, these findings pinpoint TRPV4 as an important host factor for the control of intracellular *M. tuberculosis* by macrophages, in particular when the anti-microbial potential of these cells is potentiated by IFN-γ activation.

Trpv4 Is Involved in Intracellular Trafficking of *M. tuberculosis*

Virulent mycobacteria are able to survive in resting macrophages by interfering with phagosome maturation by several mechanisms, including attenuation of intracellular calcium (Deretic and Fratti, 1999; Tejle et al., 2002), whereas IFN-γ-activated macrophages control mycobacteria, in part by promoting phagosome maturation (Ni Cheallaigh et al., 2016). We studied intracellular trafficking of mycobacteria in WT
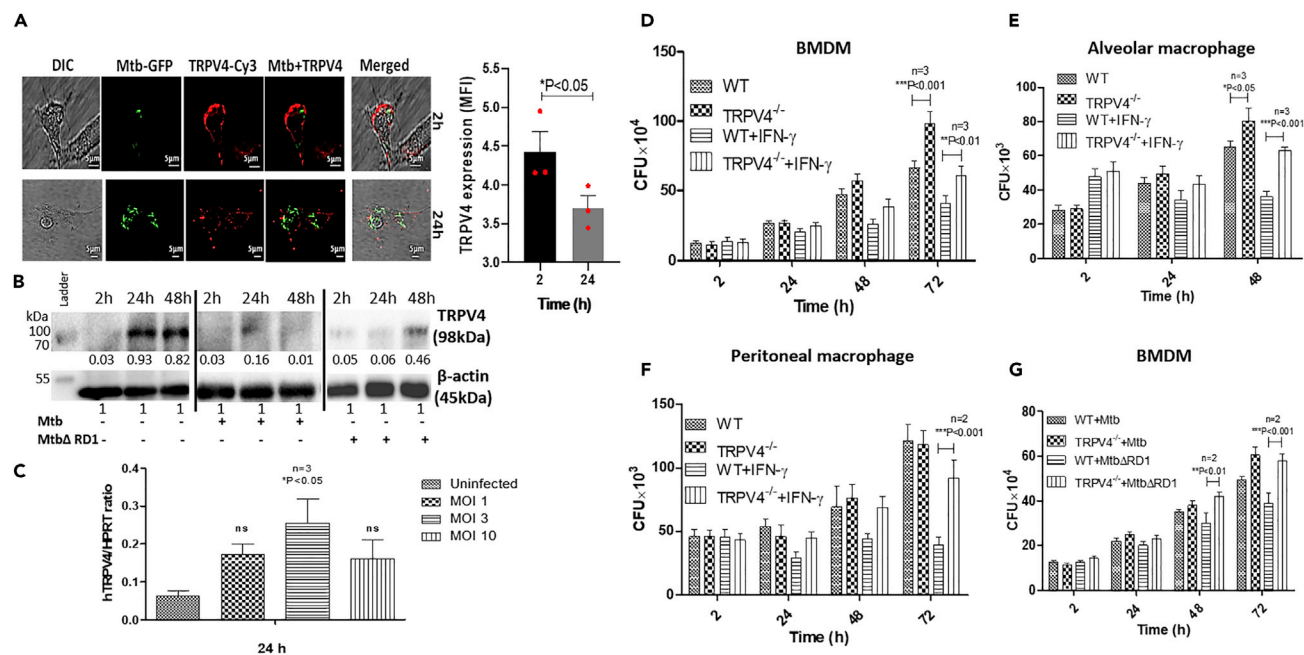
Figure 1. Trpv4 Expression and Mycobacterial Survival in Infected Macrophages

(A) Bone marrow-derived macrophages (BMDM) isolated from C57BL6/J WT mice were infected with *M. tuberculosis*-GFP (Mtb-GFP) at MOI 5, and the cells were fixed with 4% PFA 2 and 24 h p.i. TRPV4 was detected by immuno-cytochemistry using Cy3-conjugated TRPV4 antibody. Images were acquired using Leica TSC SP5 confocal microscope (scale bar = 5 μm). Mean fluorescence intensity (MFI) of TRPV4 staining was quantified by using Fiji ImageJ software. Statistical analysis was performed with two-way ANOVA. Mean ± SEM (n = 3), *p < 0.05.

(B) BMDM from C57BL6/J WT mice were infected with *M. tuberculosis*-H37Rv and *M. tuberculosis* ΔRD1 (MOI 5). Western blot analysis was performed to determine the TRPV4 expression using TRPV4-specific antibody at 2, 24 and 48 h p.i. Densitometry analysis of protein bands was performed using Fiji Image J software.

(C) Human monocyte-derived macrophages were infected with *M. tuberculosis*-H37Rv for 24 h at different MOI as indicated, and the mRNA level of *TRPV4* was studied with respect to the reference gene HPRT (hypoxanthine-guanine phosphoribosyltransferase).

(D–F) BMDM (D), alveolar macrophages (E), and peritoneal macrophages (F) were isolated from WT and *Trpv4*$^{-/-}$ mice; pre-treated with IFN-γ (500 units/mL) overnight; and then infected with *M. tuberculosis* (MOI 1) for 2 h. Cells were lysed with 0.5% Triton X-100 at different time points, and the intracellular *M. tuberculosis* counts were assessed by CFU assay.

(G) WT and *Trpv4*$^{-/-}$ mice BMDM were infected with *M. tuberculosis* or *M. tuberculosis* ΔRD1, and the intracellular bacterial burden was assessed by CFU assay after cell lysis with 0.5% Triton X-100 at indicated time points. Western blot and confocal images are representative of three independent experiments. In case of CFU assay, "n" corresponds to number of independent experiments. Statistical analysis was performed with two-way ANOVA Bonferroni post-tests. For mRNA expression of TRPV4, statistical analysis was performed with one-way ANOVA. Mean ± SD, *p < 0.05,**p < 0.01, ***p < 0.001.

versus *Trpv4*$^{-/-}$ macrophages between 5 min and 24 to 48 h p.i. *M. tuberculosis*-GFP co-localized with the early endosomal GTPase, Rab5, in both, IFN-γ-activated WT and *Trpv4*$^{-/-}$ macrophages 5 min p.i. At 24 h p.i., mycobacteria in *Trpv4*$^{-/-}$ macrophages were still mostly co-localizing with Rab5, indicating retention in early phagosomes in the absence of *Trpv4*, whereas mycobacteria-containing phagosomes in WT macrophages were Rab5 negative (Figures 2A, 2B, and S2A). In line with this view, *M. tuberculosis*-H37Rv were found in LysoTracker-positive compartments in IFN-γ-activated WT macrophages 48 h p.i. but only to a small extent in *Trpv4*$^{-/-}$ BMDM (Figures 2C and S2B). These results indicate that in the absence of *Trpv4*, IFN-γ-activated macrophages failed to effectively deliver *M. tuberculosis* into acidic phago-lyso-somal compartments.

The influence of TRPV4 on phagosome maturation was further analyzed by determining the phagosomal pH in WT and *Trpv4*$^{-/-}$ macrophages upon uptake of non-viable model particles, i.e., fluorescein isothio-cyanate (FITC)-labeled paraformaldehyde (PFA)-fixed (PF) *E. coli*. We employed the pH-sensitive property of FITC, which is quenched at acidic pH when excited at 490 nm, but not at 440 nm (Nunes et al., 2015). In TRPV4-deficient macrophages, acidification of PF *E. coli* phagosomes was significantly delayed when compared with WT cells (Figure 2D). These results demonstrate that *Trpv4* plays a crucial role in phago-some acidification and maturation, which are important prerequisites to control intracellular pathogens.
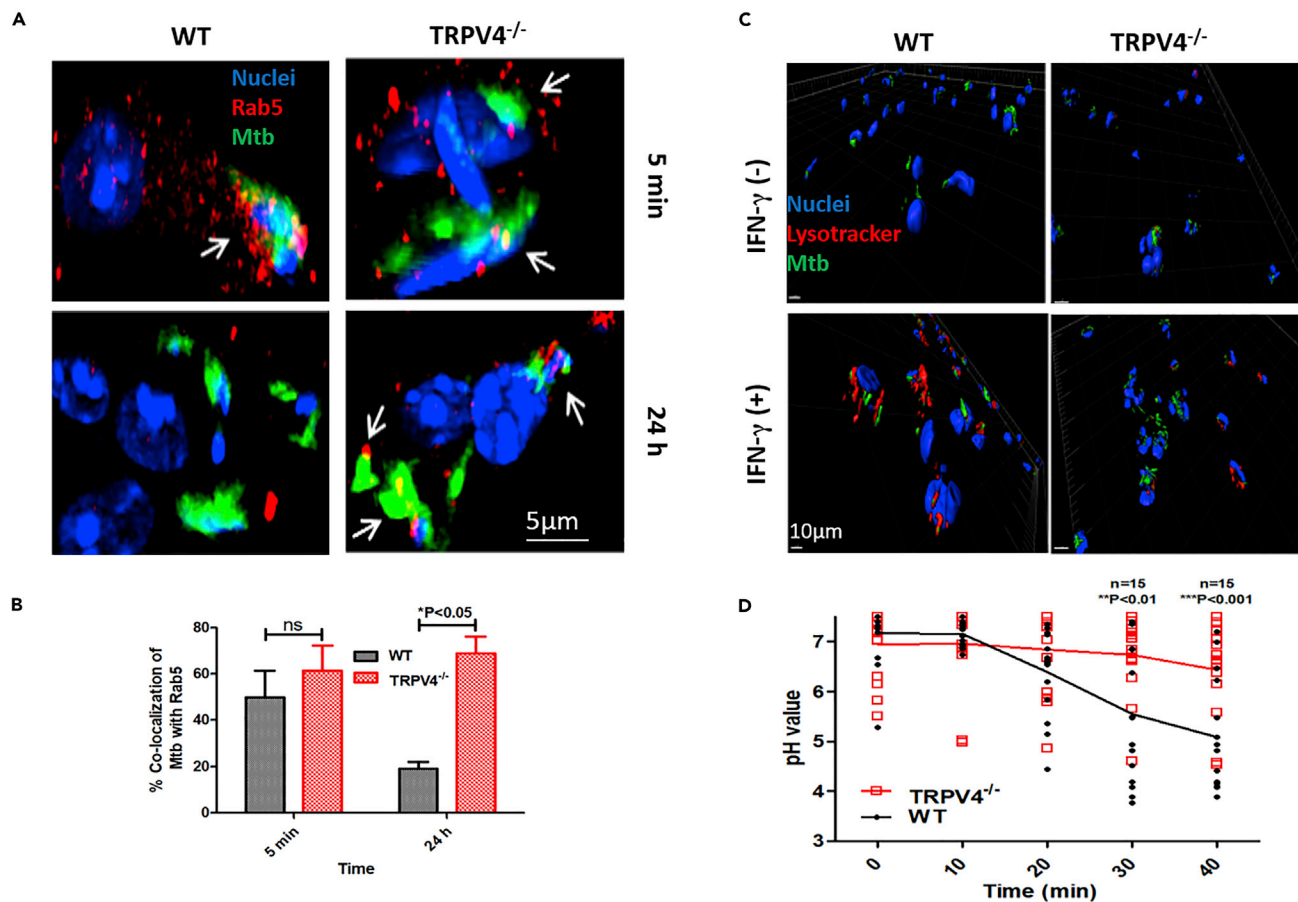
Figure 2. Localization of *M. tuberculosis* and Intracellular pH Measurement in BMDM Isolated from WT and *Trpv4*$^{-/-}$ Mice

(A) WT and *Trpv4*$^{-/-}$ BMDM were pre-treated with IFN-γ (500 units/mL) overnight. Cells were infected with *M. tuberculosis*-GFP (MOI 5), fixed with 4% PFA at indicated time points, and co-localization of *M. tuberculosis* with Rab5 (arrow marked) was studied using Rab5-specific antibody under Leica TSC SP5 confocal microscope. Images were processed with IMARIS software (Scale bar = 5 μm).

(B) At least 100 cells were analyzed to quantify the *M. tuberculosis* and Rab5 co-localization.

(C) IFN-γ-stimulated or unstimulated WT and *Trpv4*$^{-/-}$ mice BMDM were infected with *M. tuberculosis*-GFP (MOI 5). LysoTrackerRed (100nM) was added to the cells 48 h p.i., incubated for 1 h in dark at 37°C and 5% CO_2, and fixed with 4% PFA. Colocalization of *M. tuberculosis*-GFP and lysosome was studied using Leica TCS SP5 confocal microscope, and images were processed with IMARIS software (Scale bar = 10 μm).

(D) WT and *Trpv4*$^{-/-}$ BMDM were incubated with PFA-fixed FITC-labeled *Escherichia coli,* and live-cell imaging was performed by confocal microscopy with 488- and 458-nm filter to track *E. coli* containing phagosome. Phagosomal pH was measured according to pH sensitivity of FITC at ratio 488/458 nm. Experiments were performed under live-cell imaging system with TSC SP5 confocal microscope. "n" corresponds to number of FITC-*E. coli*-containing phagosomes. Statistical analysis was performed with two-way ANOVA Bonferroni post-tests. Experiments were performed in triplicates. Mean ± SD, *p < 0.05, **p < 0.01, ***p < 0.001.

Trpv4 Influences Generation of Reactive Nitrogen Species and Cell Death upon *M. tuberculosis* Infection

RNS production and apoptotic cell death represent anti-mycobacterial effector mechanisms of IFN-γ-activated macrophages controlling *M. tuberculosis,* at least in mice. It has been shown before that activation of TRPV4 induces RNS production in macrophages (Hamanaka et al., 2010). Therefore, we measured NO_2^- production of IFN-γ-activated WT and *Trpv4*$^{-/-}$ BMDM in response to either WT or ΔRD1 *M. tuberculosis*-H37Rv (MOI 5) 24 h p.i. When compared with WT macrophages, we found significantly less nitrite in *Trpv4*$^{-/-}$ ones upon infection with either WT or ΔRD1 *M. tuberculosis* (Figure 3A), which correlated with enhanced intracellular survival of *M. tuberculosis* in *Trpv4*$^{-/-}$ macrophages (Figure 1G).

Intracellular growth of *M. tuberculosis* drives host cell death through oxidative stress-mediated genomic instability (Mohanty et al., 2016). Therefore, we employed Sytox green to assess necrotic cell death in
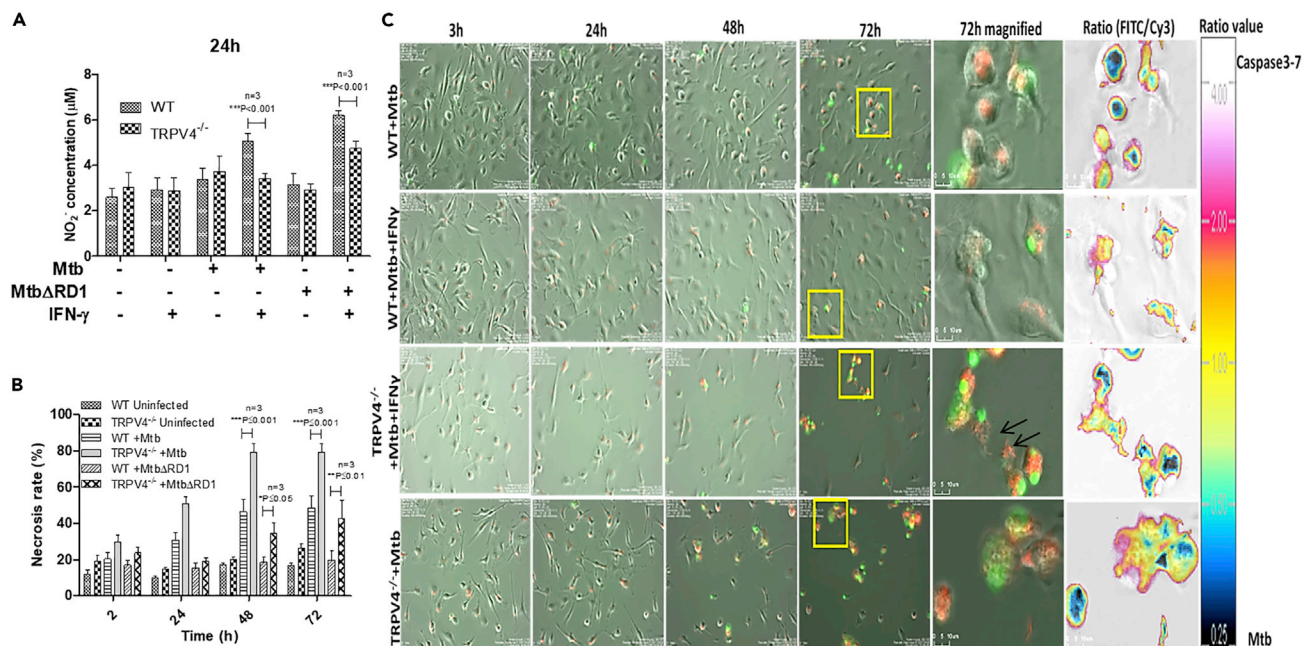
Figure 3. Determination of Nitrite Production and Cell Death in Mycobacteria-Infected WT and *Trpv4*⁻/⁻ Mice BMDM

(A) WT and *Trpv4*⁻/⁻ BMDM were incubated with or without IFN-γ overnight. Then cells were infected with *M. tuberculosis* or *M. tuberculosis* ΔRD1, and nitrite (NO_2^-) production was measured by Griess reagent after 24 h of infection using Biotek multiplate reader.

(B) BMDM were infected with *M. tuberculosis* or *M. tuberculosis* ΔRD1 (MOI 5), and cell death was studied by Sytox green (5 μM) assay with a fluorescence Ex/Em of 504/523 nm.

(C) WT and *Trpv4*⁻/⁻ BMDM were incubated with or without IFN-γ overnight and infected with *M. tuberculosis*-DsRed. After 3 h of infection, extracellular bacteria were removed by washing, and 10 μM CellEvent caspase3/7 detection reagent in DMEM media was added. Live-cell imaging for 72 h was performed using the biostation imaging system. *M. tuberculosis*-DsRed (red), and caspase3/7 activity (green) was acquired in Cy3 and FITC channel, respectively. Arrows indicates *M. tuberculosis* (red) in the extracellular environment after cell death (Scale bar of magnified image = 10 μm). Each experiment was performed in triplicate. Statistical analysis was performed with two-way ANOVA Bonferroni post-tests. Mean ± SD, *p < 0.05,**p < 0.01, ***p < 0.001.

WT versus *Trpv4*⁻/⁻ BMDM upon infection with WT or ΔRD1 *M. tuberculosis*. We observed significantly higher amounts of DNA released from the cells indicating necrotic cell death in both WT and ΔRD1 *M. tuberculosis*-infected *Trpv4*⁻/⁻ macrophages when compared with WT cells. Of note, even the ΔRD1 *M. tuberculosis* mutant, which usually causes apoptotic rather than necrotic macrophage cell death, led to higher necrosis rates in *Trpv4*⁻/⁻ than in WT macrophages (Figure 3B). To monitor cell death kinetics, we performed live-cell imaging of IFN-γ-activated *M. tuberculosis*-H37Rv-infected BMDM incubated with the fluorogenic caspase3/7 substrate as indicator for apoptosis between 3 and 72 h p.i. (Figure 3C, and Video S1). *Trpv4*⁻/⁻ macrophages succumbed much earlier, i.e., between 24 and 48 h p.i., to *M. tuberculosis* infection likely due to higher intracellular mycobacterial burden. Removal of dead cell aggregates by bystander macrophages eventually resulted in higher rates of cell death in *Trpv4*⁻/⁻ cell cultures when compared with WT ones. Notably, we also observed non-apoptotic cell death independent of caspase3/7-mediated apoptosis corroborating the necrotic cell death results shown in Figure 3B and Video S1. Taken together, these data indicate that intact TRPV4 protects host cells from *M. tuberculosis*-induced cell death.

Role of *Trpv4* in the Restriction of *M. tuberculosis* Growth in Infected Mice

Next, we investigated the role of *Trpv4 in vivo* during *M. tuberculosis* infection. Upon aerosol infection with *M. tuberculosis*-H37Rv (100 colony-forming unit [CFU]), no significant differences in the survival rates of WT and *Trpv4*⁻/⁻ mice were observed during an observation period of up to 150 days p.i. (data not shown). Body weight analysis showed no difference between infected and non-infected WT mice up to 90 days p.i. In contrast, reduced weight gain was observed in *M. tuberculosis*-infected *Trpv4*⁻/⁻ mice of the same age starting at day 21 p.i. when compared with uninfected ones (Figure 4A). It should be noted that uninfected *Trpv4*⁻/⁻ mice, when compared with WT ones, continued to gain weight over a 7-week observation period.
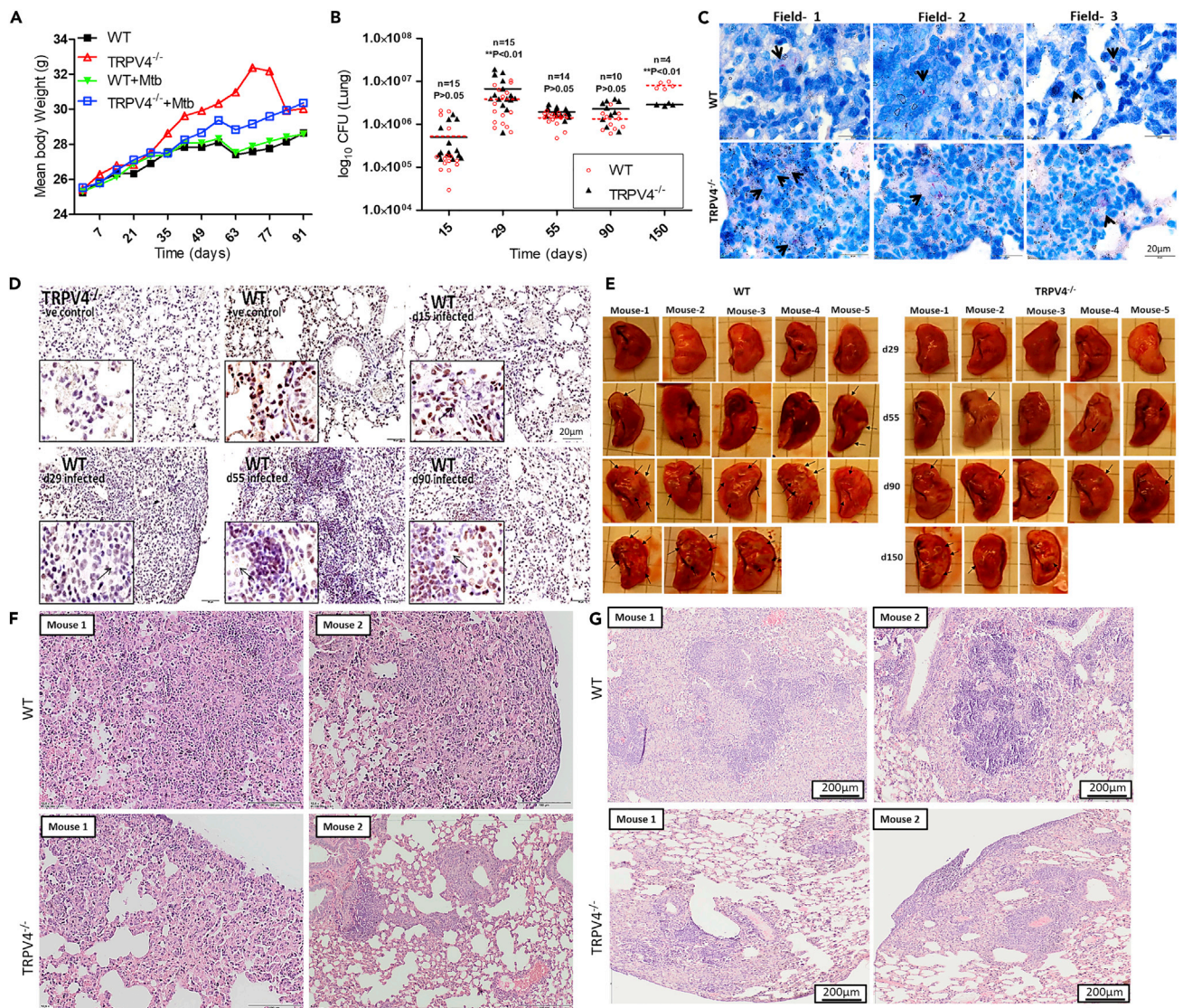
Figure 4. Determination of *M. tuberculosis*-H37Rv Survival in WT and *Trpv4*⁻/⁻ Mice

(A) Body weights of *M. tuberculosis*-H37Rv-infected and uninfected WT and *Trpv4*⁻/⁻ mice were measured during the course of infection and presented as mean weight in g.

(B) WT and *Trpv4*⁻/⁻ mice were exposed to *M. tuberculosis* aerosols (100 CFU), and bacterial burden in lungs was assessed at indicated time points by CFU assay. "n" indicates number of mice. Each point corresponds to one mouse. Statistical analysis was performed with two-way ANOVA Bonferroni post-tests. **p < 0.01.

(C) Acid fast staining was performed to determine the *M. tuberculosis* (pink and arrow marked) burden in infected WT and *Trpv4*⁻/⁻ mice lungs at day 29 p.i. Images were taken from three different fields (scale bar= 20 μm).

(D) *M. tuberculosis*-infected lung sections from WT mice were prepared at indicated time points after infection, immune-stained with Trpv4 antibody (ACC034 Alomone lab 1:200), and then developed with oxidation of 3,3′-diaminobenzidin (DAB) staining (brown) to check Trpv4 expression. Uninfected *Trpv4*⁻/⁻ and WT lung sections were used as negative and positive controls, respectively (scale bar of magnified image= 20 μm).

(E–G) (E) Lung lesions (indicated by arrow) in *M. tuberculosis*-infected WT and *Trpv4*⁻/⁻ mice are depicted for the different time points p.i. H & E staining of (F) day 29 and (G) day 55 post *M. tuberculosis*-infected WT and *Trpv4*⁻/⁻ mice lung section indicates immune cell infiltration. Images were acquired with Olympus BX41 light microscope with 10X magnification.

At 29 days p.i., both, CFU and Ziel-Nielssen's staining showed higher *M. tuberculosis* counts in *Trpv4*⁻/⁻ lungs than in WT ones (Figures 4B and 4C). At day 55 and 90 p.i. both, WT and *Trpv4*⁻/⁻ mice were similarly able to control the mycobacteria. To our surprise, significantly lower *M. tuberculosis* counts were found in lungs from *Trpv4*⁻/⁻ mice at day 150 p.i. when compared with lungs from WT animals. In spleens of *Trpv4*⁻/⁻ mice, we also found less *M. tuberculosis* counts at day 150 p.i. when compared with WT ones, despite
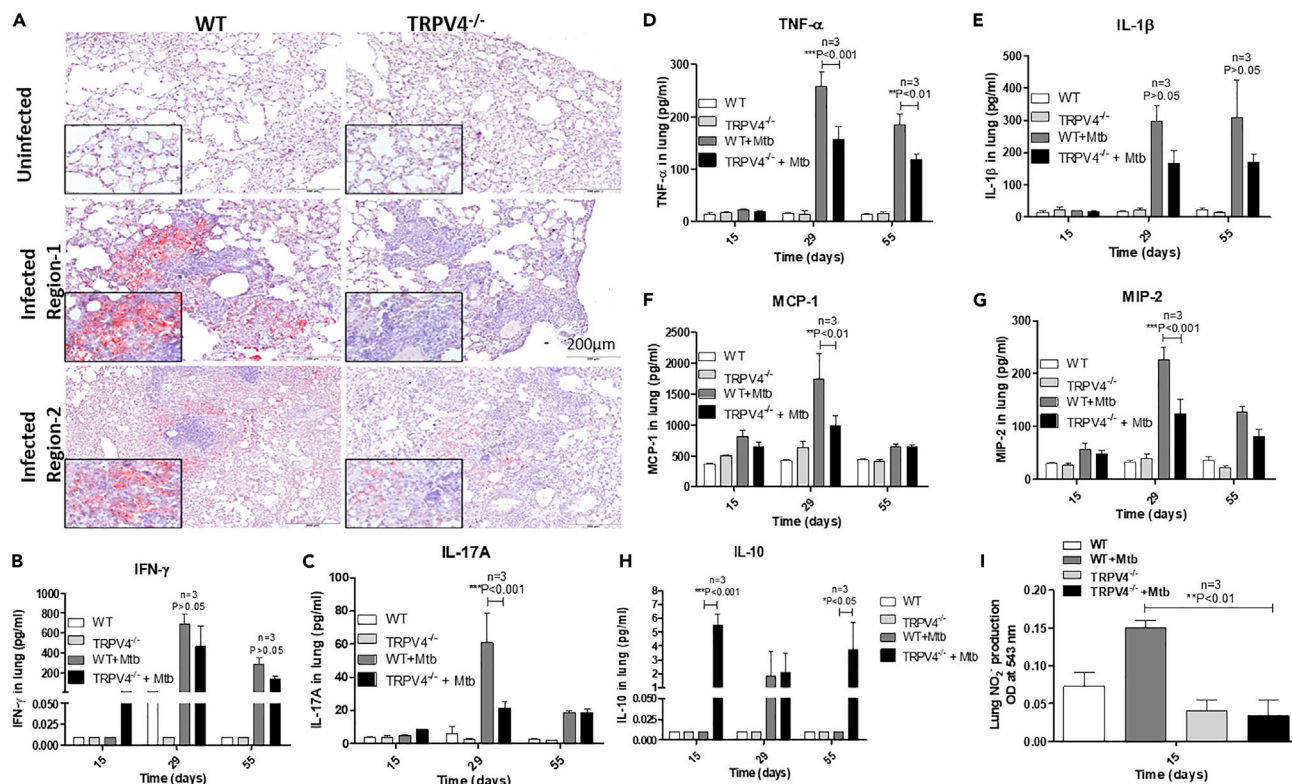
Figure 5. Analysis of Lipid Bodies, Cytokine, Chemokine, and Nitrite Production in *M. tuberculosis*-Infected WT and *Trpv4*$^{-/-}$ Mice

(A) Lipid staining of lung sections obtained from WT and *Trpv4*$^{-/-}$ mice was performed using oil red O at day 55 post infection (nuclei, blue; lipid bodies, red). Lung lysates from *M. tuberculosis*-infected WT and *Trpv4*$^{-/-}$ mice were prepared at different time points (Scale bar = 200 μm).

(B–H) Protein estimation was performed to ensure use of equal protein concentration in analysis. The production of (B) IFN-γ, (C) IL-17A, (D) TNF-α, (E) IL-1β, (F) MCP-1, (G) MIP-2, and (H) IL-10 were determined using MSD assay kit.

(I) Nitrite production was measured in lung lysates prepared from *M. tuberculosis*-infected WT and *Trpv4*$^{-/-}$ mice at 15 day p.i. using nitrate reductase and Griess reagent. The NO_2^- production was represented as the absorbance of Griess reagent at 543 nm. "n" corresponds to number of mice. Statistical analysis was performed with two-way ANOVA Bonferroni post-tests. Mean ± SEM, *p < 0.05, **<p < 0.01, ***p < 0.001.

almost similar counts at earlier time points p.i. (Figure S3A). No significant differences in mycobacterial counts between WT and *Trpv4*$^{-/-}$ mice were seen in the livers during the entire course of infection (Figure S3B). Immuno-histological analysis of WT lungs showed TRPV4-expressing cells at the periphery of granuloma, whereas cells present in the center showed reduced TRPV4 expression (arrow marked) (Figure 4D). Pulmonary inflammatory lesions (arrow marked) were larger in WT compared with *Trpv4*$^{-/-}$ mice at days 55, 90, and 150 p.i. (Figure 4E). H&E staining revealed larger areas of inflammatory infiltrates at the site of infection in *M. tuberculosis*-infected WT mouse lungs at day 29 (Figure 4F) and day 55 (Figure 4G) p.i. when compared with *M. tuberculosis*-infected *Trpv4*$^{-/-}$ mouse lungs. These data indicate that TRPV4 is involved in the immune responses, which control *M. tuberculosis* burden in mice, however, with opposite functions, i.e., protective versus pathological, in the early versus late stage of infection.

M. tuberculosis utilizes host lipid droplets as nutrient source for growth in granulomas (Daniel et al., 2011). Using oil red O staining of lung tissue sections, we already noticed more lipid droplets in lungs from uninfected WT mice when compared with *Trpv4*$^{-/-}$ones (Figure S3D). More importantly, at day 55 p.i., *M. tuberculosis*-infected WT mice showed intense accumulation of lipid bodies in the lungs, which was more pronounced when compared with *Trpv4*$^{-/-}$mice (Figures 5A and S3C).

Reduced Pro-inflammatory Responses in *Trpv4*$^{-/-}$ Mice upon *M. tuberculosis* Infection

Infiltration of immune cells to the site of infection is crucial for the restriction of *M. tuberculosis* growth *in vivo*. Analysis of a panel of cytokines and chemokines in lung lysates of *M. tuberculosis*-infected mice showed higher production of the pro-inflammatory cytokines, IFN-γ, IL-17A, TNF-α, and IL-1β in WT
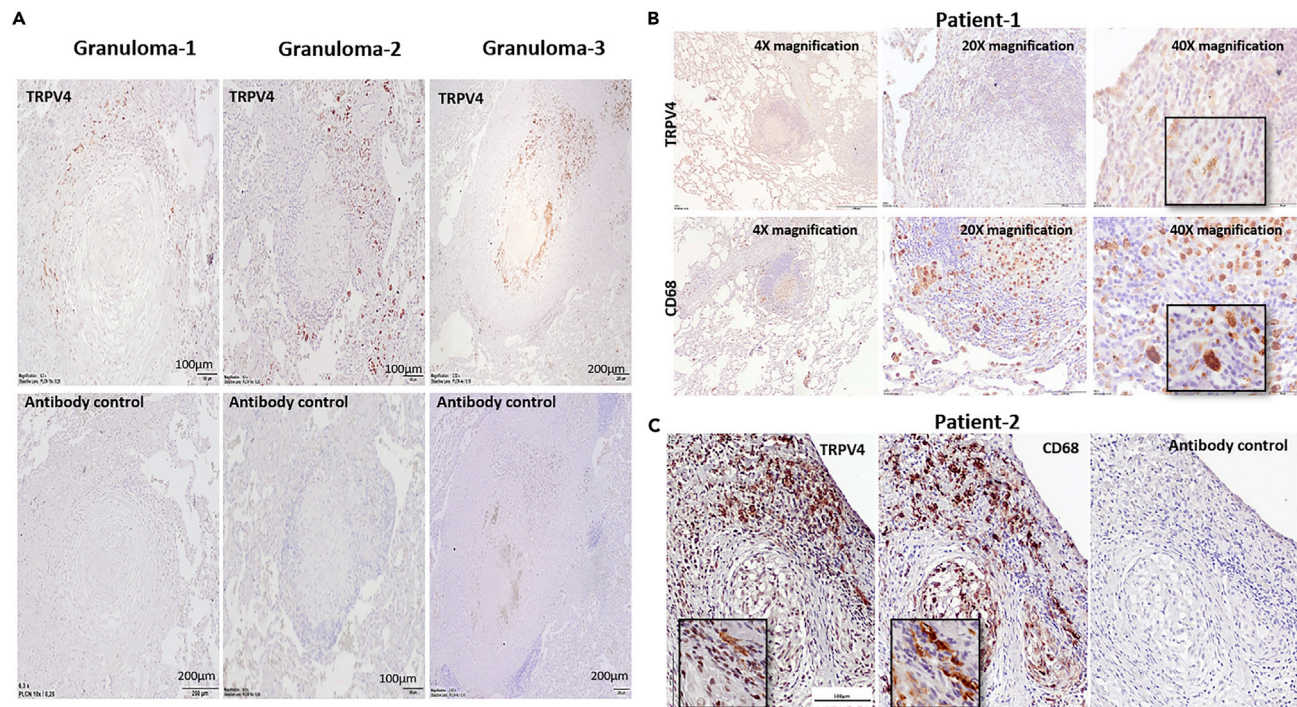
Figure 6. Analysis of TRPV4 Expression in Lung Granulomas of a Patient with TB

Lung tissue sections were obtained from patients with TB, who underwent anti-TB therapy and lung tissue resection as part of the treatment.

(A) Immunohistochemistry was performed using an antibody to TRPV4, followed by a species-specific secondary antibody and DAB development (TRPV4, brown; nuclei, blue).

(B and C) Human lung tissue sections of patients with TB were stained for TRPV4 and CD68 and developed by DAB staining showing expression of TRPV4 and CD68 in TB granuloma (TRPV4 and CD68, brown; nuclei, blue; Scale bar = 100 μm).

than in $Trpv4^{-/-}$ mice. IFN-γ production was enhanced in both, WT and $Trpv4^{-/-}$ compared with uninfected mice, although WT mice showed moderately higher IFN-γ production than $Trpv4^{-/-}$ ones (Figure 5B). We also observed higher concentrations of IL-17A, TNF-α, and IL-1β in WT than in TRPV4$^{-/-}$ lungs at day 29 p.i. (Figures 5C–5E). Upon infection, the production of keratinocyte chemoattractant (KC) was increased in WT when compared with $Trpv4^{-/-}$ lungs, whereas IL-6 secretion was only moderately but not significantly enhanced (Figures S4A and S4B). Similarly, we observed higher concentrations of the chemokines, monocyte chemoattractant protein-1 (MCP-1), and macrophage inflammatory protein 2 (MIP-2 or CXCL2) in lungs from WT when compared with those from $Trpv4^{-/-}$ mice (Figures 5F and 5G). In contrast, the anti-inflammatory cytokine, IL-10, was significantly increased in $Trpv4^{-/-}$ lung tissue samples taken at day 15 and, again, at day 55 p.i. when compared with WT lungs. Comparable IL-10 concentrations were observed at day 29 p.i. (Figure 5H).

Determination of NO_2^- production at day 15 p.i. with *M. tuberculosis* showed enhanced NO_2^- concentrations in the lungs from WT but not $Trpv4^{-/-}$ mice. No differences in nitrite concentrations were observed in serum samples (Figures 5I and S4C).

Differential TRPV4 Distribution in Granulomas from Patients with TB

To investigate whether TRPV4 is also present in granulomas of human patients with TB, we analyzed TRPV4 expression in tissue section of lung granulomas obtained from three patients with TB, who had undergone lung tissue resection. We observed more TRPV4-positive cells at the periphery of the granuloma in all three patients, whereas cells in the center showed much weaker TRPV4 signals (Figure 6A). Dual staining with antibodies against the CD68 macrophage marker and TRPV4 in consecutive sections showed that TRPV4 expression did partially overlap with CD68-positive macrophages but was also associated with CD68-negative cells. CD68-positive cells present at the periphery of granulomas expressed more TRPV4, whereas those present at the center of the granuloma showed less TRPV4 (Figures 6B and 6C).
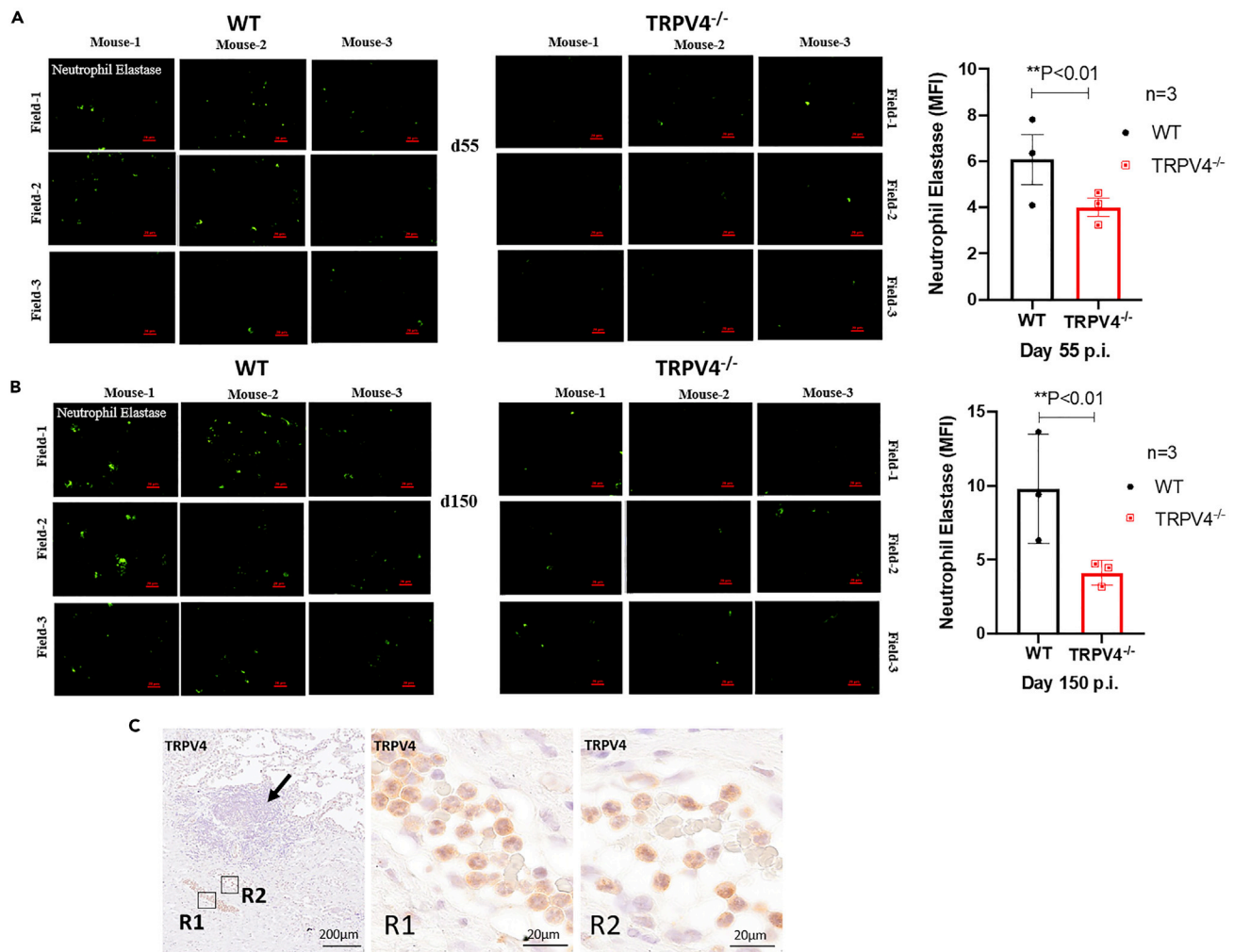
Figure 7. Expression of Neutrophil Elastase in *M. tuberculosis*-Infected Mouse Lung

(A–C) (A and B) WT and *Trpv4*$^{-/-}$ mice were infected with *M. tuberculosis* (100 CFU) via aerosol, and 4-μm cryosections of lung tissue samples were prepared after days 55 and 150 p.i. Tissue sections were stained by fluorescence immunohistochemistry assay for neutrophil elastase (green). Images were acquired from three different zones of infection (field) from each mouse; Scale bar=20 μm). Mean fluorescence intensity (MFI) of neutrophil elastase staining was quantified by using Fiji ImageJ software. (C) Human lung tissue sections of patients with TB were stained for TRPV4 showing positive signals in polymorphonuclear neutrophils in a blood vessel at the site of infection (Scale bar of R1, R2 = 20 μm).

Neutrophils represent the predominant cell population infected with *M. tuberculosis* in pulmonary samples from patients with active TB and are thought to fail controlling the infection and rather drive exacerbation of inflammation (Dallenga et al., 2017; Eum et al., 2010). Using immunofluorescence staining for neutrophil elastase (NE), we observed increasing numbers of NE-positive neutrophils in lungs from *M. tuberculosis*-infected WT mice between day 55 and 150 p.i., whereas only few NE signals were found in *Trpv4*$^{-/-}$ lungs (Figures 7A and 7B). Notably, we also observed TRPV4-positive neutrophil aggregates in blood vessels in close proximity to the granulomatous tissue from patients with active TB (Figure 7C). In summary, TRPV4 in human TB lesions was primarily associated with macrophages and neutrophils, and in mice, recruitment of neutrophils was reduced in the absence of TRPV4 at later time points of *M. tuberculosis* infection, indicating a link between TRPV4 expression and neutrophil-associated inflammation.

DISCUSSION

In immune cells, different ion channels such as voltage-gated calcium channels, non-selective calcium channel, and transient receptor potential (TRP) ion channels are crucial for the regulation of calcium levels to facilitate cellular signaling pathways and effector functions (Song et al., 2015). Here, we report that

virulent, but not attenuated *M. tuberculosis,* down-regulated *Trpv4* expression in murine macrophages, indicating that *M. tuberculosis* can interfere with TRPV4 function. Importantly, we revealed that *M. tuberculosis*-regulated *Trpv4* expression may critically be involved in modulating TB disease progression. In the absence of *Trpv4*, resting but even more prominently, IFN-γ activated $Trpv4^{-/-}$ macrophages failed to control growth of intracellular *M. tuberculosis*. This *in vitro* susceptibility phenotype corresponded to the failure of $Trpv4^{-/-}$ mice in restricting pulmonary mycobacterial numbers in the early stage of infection during the growth phase of *M. tuberculosis*. In contrast, the lack of *Trpv4* was associated with better control of mycobacteria at the later chronic stage of infection. Thus, TRPV4 has a biphasic function associated with an early protective but later permissive phenotype. Association of functional TRPV4 with higher susceptibility to *M. tuberculosis* at later stages of infection in the murine TB model was paralleled by the presence of TRPV4-expressing macrophages and neutrophils in the periphery of granulomas from chronically infected WT mice and patients with active TB.

As a hallmark of *M. tuberculosis* virulence, the pathogen is able to inhibit phagosome acidification, a prerequisite for phagosome maturation and phago-lysosome fusion (Wong et al., 2011). We found that, at 24 h p.i., WT but not ΔRD1 *M. tuberculosis* infection moderately reduced intracellular calcium levels in WT macrophages, indicating that *M. tuberculosis* virulence genes encoded by the RD1 region are important for TRPV4 down-regulation and hence, reduction of calcium ion concentration, which otherwise is a prerequisite for phago-lysosome fusion (Figures S4D and S4E). Thereby, *M. tuberculosis* is able to maintain an immature phagosomal state as niche for intracellular growth, even in IFN-γ-activated macrophages (Trimble and Grinstein, 2007). This notion is supported by the retention of Rab-5 in *M. tuberculosis* phagosomes in TRPV4-deficient macrophages. This is not seen in mycobacterial phagosomes of WT macrophages, which efficiently delivered WT *M. tuberculosis* into phago-lysosomes. In fact, we also observed lower calcium uptake in resting $Trpv4^{-/-}$ compared with WT macrophages when incubated with ionomycin Ca^{2+} (Figure S4F). Increased cytosolic calcium levels enhance phagosome acidification. Accordingly, inhibition of calcium signaling by *M. tuberculosis* can interfere with phago-lysosome fusion, thereby promoting the pathogen's intracellular survival (Malik et al., 2000). Beyond mycobacteria, hampered phagosome maturation in the absence of TRPV4 seems a general phenotype as acidification of phagosomes containing fixed *E. coli* cells was also delayed. Taken together, our results suggest that virulent *M. tuberculosis,* in addition to other virulence mechanisms, target *Trpv4,* thereby impairing phagosome acidification and maturation to secure intracellular survival and growth. To see whether the *in vitro* susceptibility phenotype of $Trpv4^{-/-}$ macrophages is also relevant for bacterial infections other than mycobacterial ones, we infected WT versus $Trpv4^{-/-}$ BMDM with *Salmonella typhimurium*. In contrast to mycobacteria, the salmonellae grew similarly in WT and $Trpv4^{-/-}$ macrophages (data not shown), indicating that the observed phenotype is mycobacteria specific.

M. tuberculosis infection promotes apoptosis of human alveolar macrophages (Keane et al., 1997). Staining for active caspase3/7 revealed that $Trpv4^{-/-}$ macrophages infected with *M. tuberculosis* succumbed to apoptotic cell death earlier than WT cells, which was likely due to higher intracellular mycobacterial burden 36 h p.i. Using live-cell imaging, we observed that apoptotic cells were engulfed by bystander macrophages leading to removal of more than 90% $Trpv4^{-/-}$ macrophages by 72 h p.i. These results indicate a relevance of *Trpv4* in *M. tuberculosis*-mediated host cell death.

Aerosol infection of $Trpv4^{-/-}$ mice and their WT littermates with *M. tuberculosis* revealed that the lack of *Trpv4* led to higher bacterial burden at day 29 p.i., but equal ones at days 55 and 90, and significantly lower ones at days 150 p.i. Reduced control of *M. tuberculosis* in mice lacking *Trpv4* in the early stage of infection is likely due to the failure of TRP4-deficient macrophages to promote phagosome maturation and RNS production. Moreover, inflammatory responses were reduced in $Trpv4^{-/-}$ lungs when compared with WT littermates including smaller inflammatory infiltrates and granuloma-like structures at the site of infection. This could be due to lower concentrations of MCP-1 and MIP-2, which are involved in the recruitment of immune cells to the infection sites, in *M. tuberculosis*-infected $Trpv4^{-/-}$ versus WT lungs (Figures 4F and 4G), which corroborates previous observations (Ye et al., 2012). IFN-γ and IL-17 production was increased in lungs of WT, but not of $Trpv4^{-/-}$, mice at day 29 post *M. tuberculosis* infection and associated with reduced TNF-α production otherwise important for optimal macrophage activation. These data suggest that $Trpv4^{-/-}$ mice failed to develop sufficient innate immune responses to combat *M. tuberculosis*. In contrast, enlarged lung lesions and higher concentrations of pro-inflammatory cytokines and effectors produced in WT when compared with $Trpv4^{-/-}$ mice were likely instrumental in

controlling *M. tuberculosis* growth in the presence of *Trpv4*. Increased secretion of the anti-inflammatory cytokine, IL-10, in *Trpv4*$^{-/-}$ versus WT mice infected with *M. tuberculosis* is likely responsible for this reduced Th1 response observed. Enhanced influx of neutrophils in WT compared with TRPV4$^{-/-}$ mice at the later stage of infection is likely contributing to enhanced inflammation in the presence of TRPV4. Inhibited TRPV4 has been shown to limit neutrophil functions including chemotaxis (Yin et al., 2016). Excessive secretion of neutrophil elastase by activated neutrophils is involved in the control of *M. tuberculosis,* but at the same time, can also cause tissue damage and pathology. Thus, TRPV4 has a protective role in *M. tuberculosis* infection during the early innate immune response phase before T cell immunity kicks in, but a detrimental one later in infection when exacerbated inflammatory responses including neutrophil influx maintain mycobacterial growth.

The appearance of lipid-storing macrophages as characterized by lipid droplets (LD) is a histopathological hallmark of the chronically *M. tuberculosis*-infected murine lung later in infection. LD formation in *M. tuberculosis*-infected macrophages has been suggested to be a programmed host response coordinated by IFN-γ (Knight et al., 2018). However, *M. tuberculosis* can utilize fatty acids stored in LDs as carbon source for intracellular growth. Thus, our observation that pulmonary lesions in *Trpv4*$^{-/-}$ mice contained less LDs than those in WT mice may also account for lower mycobacterial loads in *Trpv4*$^{-/-}$ compared with WT lungs at late stage of infection, i.e., day 150. This phenotype is likely caused by a reduced IFN-γ and neutrophil-driven inflammatory environment promoted by enhanced IL-10 production in the absence of *Trpv4*. Apart from providing a food source for mycobacteria, LDs are also involved in the production of pro-inflammatory eicosanoids such as prostaglandin E$_2$, which promote neutrophil influx into the infected tissue. As such, lower numbers of LDs in lungs of *M. tuberculosis*-infected *Trpv4*$^{-/-}$ mice might be responsible for reduced inflammatory responses and neutrophil aggregations when compared with WT lungs (Kaul et al., 2012; Saka and Valdivia, 2012).

The relevance of TRPV4 in *M. tuberculosis* infection identified by our experimental studies in mice prompted us to analyze its presence in human TB lesions. Immuno-histopathological analyses of lung granuloma sections from three patients with TB showed TRPV4-expressing macrophages at the periphery of the necrotic granuloma, whereas those in the centers showed less TRPV4 expression. Exposure of macrophages to *M. tuberculosis* and its metabolites, which happens more likely in the center of TB granulomas, as well as subsequent necrotic cell death may account for the reduced TRPV4 expression observed. It should, however, be noted that the patients with TB, from which the tissue samples were derived, had a history of long-term anti-TB treatment. Nevertheless, surgery was needed to overcome prolonged culture positivity and imminent treatment failure. Consequently, bacterial loads through acid-fast staining could not be visualized despite the strong and obvious granulomatous lesions present. Notably, TRPV4 was also observed in neutrophils in the granuloma-adjacent blood vessels. This finding supports previous reports that TRPV4 deficiency impairs neutrophil response to pro-inflammatory stimuli, production of reactive oxygen species, adhesion, and chemotaxis (Yin et al., 2016).

Taken together, we report a novel bifunctional role of the TRPV4 ion channel in host responses to *M. tuberculosis* infection in mice, in which TRPV4 is protective during the early innate but exacerbating and proinflammatory during the late chronic stage of infection. To this end, the presence of TRPV4-expressing myeloid cells in lung granulomas indicates TRPV4 as a potential target to be explored for host-directed therapy to control TB disease progression and support antibiotic treatment.

Limitations of the Study

In this study, although we have observed down-regulation of TRPV4 by pathogenic *M. tuberculosis* H37Rv in macrophages, we believe that TRPV4 expression can also be regulated by other intracellular factors during *in vitro* culture in the absence of an infectious stimulus (Figure 1B uninfected condition). In our follow-up studies, we will compare TRPV4 expression in different innate and acquired immune cell populations from un-infected versus infected mice to delineated regulatory mechanisms, as well as the kinetics of immune cell frequencies during the infectious process to identify responses responsible for higher and lower susceptibility of *Trpv4*$^{-/-}$ mice early versus later in infection. Future availability of specific TRPV4 inhibitors employable *in vivo*, will allow to explore the host-directed therapy approach targeting TRPV4 in late stage of infection using a susceptible mouse model of TB. Ultimately, the cellular and molecular functions of TRPV4 and its putative interaction partners during macrophage responses to *M. tuberculosis* need to be approached using cell biology and biochemistry approaches. Our observation of a decreased neutrophil

influx in lungs of *M. tuberculosis*-infected *Trpv4*$^{-/-}$ mice late in infection also requires further investigations to understand the underlaying molecular and immunological mechanisms of how TRPV4 is involved here and how this knowledge can be explored to improve treatment of tuberculosis.

Resource Availability

Lead Contact

Further information and requests for resources and reagents should be directed to and will be fulfilled by the Lead Contact, Prof. Dr. Ulrich E. Schaible (uschaible@fz-borstel.de).

Materials Availability

This study did not generate new unique reagents.

Data and Code Availability

This study did not generate datasets/code.

METHODS

All methods can be found in the accompanying Transparent Methods supplemental file.

SUPPLEMENTAL INFORMATION

Supplemental Information can be found online at https://doi.org/10.1016/j.isci.2020.101206.

AUTHOR CONTRIBUTIONS

S.K.N. designed, performed and analyzed the experiments and wrote the manuscript; K.P. performed the experiments and analyzed the data; J.E. and V.S. provided technical assistance and training; M.H. wrote the ethical approval for animal experiment; B.K. as clinician recruited patients with TB; B.K. and N.R. provided the lung samples from patients with TB; W.L. created the *Trpv4*$^{-/-}$ mice; W.M.K. provided the *Trpv4*$^{-/-}$ mice and revised the manuscript; U.E.S. designed experiments, analyzed the data, and contributed to writing the manuscript; A.S. designed experiments, analyzed the data, obtained funding, and wrote the manuscript.

DECLARATION OF INTERESTS

The authors have no conflict of interest.

REFERENCES

Alpizar, Y.A., Boonen, B., Sanchez, A., Jung, C., Lopez-Requena, A., Naert, R., Steelant, B., Luyts, K., Plata, C., De Vooght, V., et al. (2017). TRPV4 activation triggers protective responses to bacterial lipopolysaccharides in airway epithelial cells. Nat. Commun. *8*, 1059.

Balakrishna, S., Song, W., Achanta, S., Doran, S.F., Liu, B., Kaelberer, M.M., Yu, Z., Sui, A., Cheung, M., Leishman, E., et al. (2014). TRPV4 inhibition counteracts edema and inflammation and improves pulmonary function and oxygen saturation in chemically induced acute lung injury.

Am. J. Physiol. Lung Cell. Mol. Physiol. *307*, L158–L172.

Dallenga, T., Repnik, U., Corleis, B., Eich, J., Reimer, R., Griffiths, G.W., and Schaible, U.E. (2017). M. tuberculosis-induced necrosis of

infected neutrophils promotes bacterial growth following phagocytosis by macrophages. Cell Host Microbe 22, 519–530.e3.

Daniel, J., Maamar, H., Deb, C., Sirakova, T.D., and Kolattukudy, P.E. (2011). Mycobacterium tuberculosis uses host triacylglycerol to accumulate lipid droplets and acquires a dormancy-like phenotype in lipid-loaded macrophages. PLoS Pathog. 7, e1002093.

de Jonge, M.I., Pehau-Arnaudet, G., Fretz, M.M., Romain, F., Bottai, D., Brodin, P., Honore, N., Marchal, G., Jiskoot, W., England, P., et al. (2007). ESAT-6 from Mycobacterium tuberculosis dissociates from its putative chaperone CFP-10 under acidic conditions and exhibits membrane-lysing activity. J. Bacteriol. 189, 6028–6034.

Deretic, V., and Fratti, R.A. (1999). Mycobacterium tuberculosis phagosome. Mol. Microbiol. 31, 1603–1609.

Eum, S.Y., Kong, J.H., Hong, M.S., Lee, Y.J., Kim, J.H., Hwang, S.H., Cho, S.N., Via, L.E., and Barry, C.E., 3rd (2010). Neutrophils are the predominant infected phagocytic cells in the airways of patients with active pulmonary TB. Chest 137, 122–128.

Gombedza, F., Kondeti, V., Al-Azzam, N., Koppes, S., Duah, E., Patil, P., Hexter, M., Phillips, D., Thodeti, C.K., and Paruchuri, S. (2017). Mechanosensitive transient receptor potential vanilloid 4 regulates Dermatophagoides farinae-induced airway remodeling via 2 distinct pathways modulating matrix synthesis and degradation. FASEB J. 31, 1556–1570.

Hamanaka, K., Jian, M.Y., Townsley, M.I., King, J.A., Liedtke, W., Weber, D.S., Eyal, F.G., Clapp, M.M., and Parker, J.C. (2010). TRPV4 channels augment macrophage activation and ventilator-induced lung injury. Am. J. Physiol. Lung Cell. Mol. Physiol. 299, L353–L362.

Jia, Y., Wang, X., Varty, L., Rizzo, C.A., Yang, R., Correll, C.C., Phelps, P.T., Egan, R.W., and Hey, J.A. (2004). Functional TRPV4 channels are expressed in human airway smooth muscle cells. Am. J. Physiol. Lung Cell. Mol. Physiol. 287, L272–L278.

Kaul, V., Bhattacharya, D., Singh, Y., Van Kaer, L., Peters-Golden, M., Bishai, W.R., and Das, G. (2012). An important role of prostanoid receptor EP2 in host resistance to Mycobacterium tuberculosis infection in mice. J. Infect. Dis. 206, 1816–1825.

Keane, J., Balcewicz-Sablinska, M.K., Remold, H.G., Chupp, G.L., Meek, B.B., Fenton, M.J., and Kornfeld, H. (1997). Infection by Mycobacterium tuberculosis promotes human alveolar macrophage apoptosis. Infect. Immun. 65, 298–304.

King, M.M., Kayastha, B.B., Franklin, M.J., and Patrauchan, M.A. (2020). Calcium regulation of bacterial virulence. Adv. Exp. Med. Biol. 1131, 827–855.

Knight, M., Braverman, J., Asfaha, K., and Gronert, K. (2018). Lipid droplet formation in Mycobacterium tuberculosis infected macrophages requires IFN-gamma/HIF-1alpha signaling and supports host defense. PLoS Pathog. 14, e1006874.

Malik, Z.A., Denning, G.M., and Kusner, D.J. (2000). Inhibition of Ca(2+) signaling by Mycobacterium tuberculosis is associated with reduced phagosome-lysosome fusion and increased survival within human macrophages. J. Exp. Med. 191, 287–302.

Mohanty, S., Dal Molin, M., Ganguli, G., Padhi, A., Jena, P., Selchow, P., Sengupta, S., Meuli, M., Sander, P., and Sonawane, A. (2016). Mycobacterium tuberculosis EsxO (Rv2346c) promotes bacillary survival by inducing oxidative stress mediated genomic instability in macrophages. Tuberculosis (Edinb.) 96, 44–57.

Moran, M.M., McAlexander, M.A., Biro, T., and Szallasi, A. (2011). Transient receptor potential channels as therapeutic targets. Nat. Rev. Drug Discov. 10, 601–620.

Ni Cheallaigh, C., Sheedy, F.J., Harris, J., Munoz-Wolf, N., Lee, J., West, K., McDermott, E.P., Smyth, A., Gleeson, L.E., Coleman, M., et al. (2016). A common variant in the adaptor mal regulates interferon gamma signaling. Immunity 44, 368–379.

Nunes, P., Guido, D., and Demaurex, N. (2015). Measuring phagosome pH by ratiometric fluorescence microscopy. J. Vis. Exp. e53402, https://doi.org/10.3791/53402.

Reilly, C.A., Johansen, M.E., Lanza, D.L., Lee, J., Lim, J.O., and Yost, G.S. (2005). Calcium-dependent and independent mechanisms of capsaicin receptor (TRPV1)-mediated cytokine production and cell death in human bronchial epithelial cells. J. Biochem. Mol. Toxicol. 19, 266–275.

Sabnis, A.S., Reilly, C.A., Veranth, J.M., and Yost, G.S. (2008). Increased transcription of cytokine genes in human lung epithelial cells through activation of a TRPM8 variant by cold temperatures. Am. J. Physiol. Lung Cell. Mol. Physiol. 295, L194–L200.

Saka, H.A., and Valdivia, R. (2012). Emerging roles for lipid droplets in immunity and host-pathogen interactions. Annu. Rev. Cell Dev. Biol. 28, 411–437.

Song, L., Cui, R., Yang, Y., and Wu, X. (2015). Role of calcium channels in cellular antituberculosis effects: potential of voltage-gated calcium-channel blockers in tuberculosis therapy. J. Microbiol. Immunol. Infect. 48, 471–476.

Suresh, K., Servinsky, L., Reyes, J., Baksh, S., Undem, C., Caterina, M., Pearse, D.B., and Shimoda, L.A. (2015). Hydrogen peroxide-induced calcium influx in lung microvascular endothelial cells involves TRPV4. Am. J. Physiol. Lung Cell. Mol. Physiol. 309, L1467–L1477.

Tejle, K., Magnusson, K.E., and Rasmusson, B. (2002). Phagocytosis and phagosome maturation are regulated by calcium in J774 macrophages interacting with unopsonized prey. Biosci. Rep. 22, 529–540.

Trimble, W.S., and Grinstein, S. (2007). TB or not TB: calcium regulation in mycobacterial survival. Cell 130, 12–14.

Venkatachalam, K., and Montell, C. (2007). TRP channels. Annu. Rev. Biochem. 76, 387–417.

Wong, D., Bach, H., Sun, J., Hmama, Z., and Av-Gay, Y. (2011). Mycobacterium tuberculosis protein tyrosine phosphatase (PtpA) excludes host vacuolar-H+-ATPase to inhibit phagosome acidification. Proc. Natl. Acad. Sci. U S A 108, 19371–19376.

Ye, L., Kleiner, S., Wu, J., Sah, R., Gupta, R.K., Banks, A.S., Cohen, P., Khandekar, M.J., Bostrom, P., Mepani, R.J., et al. (2012). TRPV4 is a regulator of adipose oxidative metabolism, inflammation, and energy homeostasis. Cell 151, 96–110.

Yin, J., Michalick, L., Tang, C., Tabuchi, A., Goldenberg, N., Dan, Q., Awwad, K., Wang, L., Erfinanda, L., Nouailles, G., et al. (2016). Role of transient receptor potential vanilloid 4 in neutrophil activation and acute lung injury. Am. J. Respir. Cell Mol. Biol. 54, 370–383.

Supplemental Information

Differential Roles of the Calcium Ion Channel TRPV4

in Host Responses to *Mycobacterium tuberculosis*

Early and Late in Infection

Sumanta Kumar Naik, Kaliprasad Pattanaik, Jacqueline Eich, Vivien Sparr, Matthias Hauptmann, Barbara Kalsdorf, Norbert Reiling, Wolfgang Liedtke, Wolfgang M. Kuebler, Ulrich E. Schaible, and Avinash Sonawane

Figure S1   Related to Figure 1
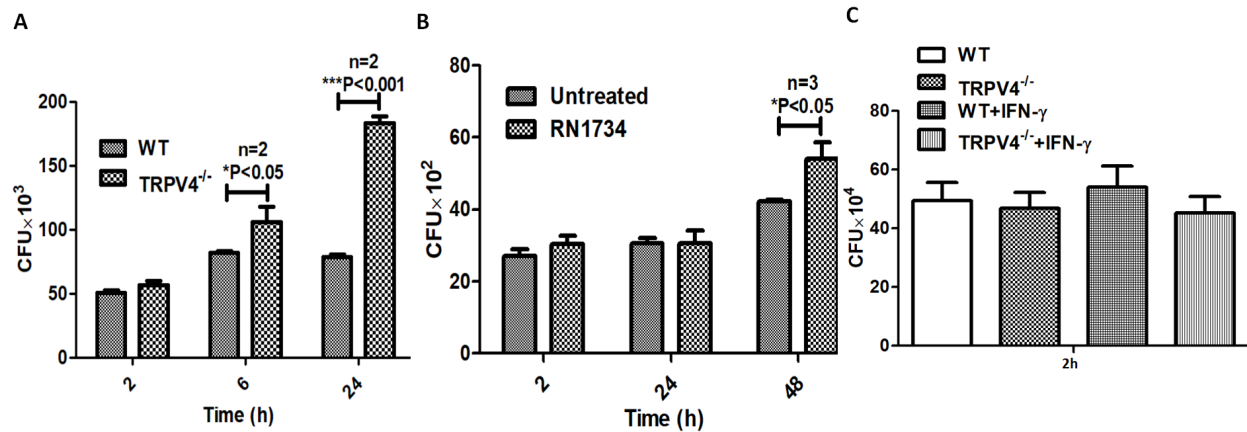
Figure S1.

(A) BMDM from WT and *Trpv4-/-* macrophages were infected with *M. smegmatis* (Msm) at a MOI 1 and intracellular bacterial counts were assessed by CFU at indicated time points p.i. **(B)** RAW264.7 macrophages were treated with the Trpv4 inhibitor, RN1734 (10μM), prior to *M. tuberculosis* infection of a MOI1. Intracellular mycobacterial counts were assessed at indicated time points by CFU assay. **(C)** BMDM from WT and *Trpv4-/-* mice were infected with *M. tuberculosis* at MOI 5 and the numbers of phagocytosed *M. tuberculosis* were assessed by CFU at 2h p.i. Data represent the mean ± SEM from 2 - 3 (n) independent experiments. Statistical analysis was performed with Two Way ANOVA Bonferroni posttests. *P<0.05, ***P<0.001.

Figure S2   Related to Figure 2
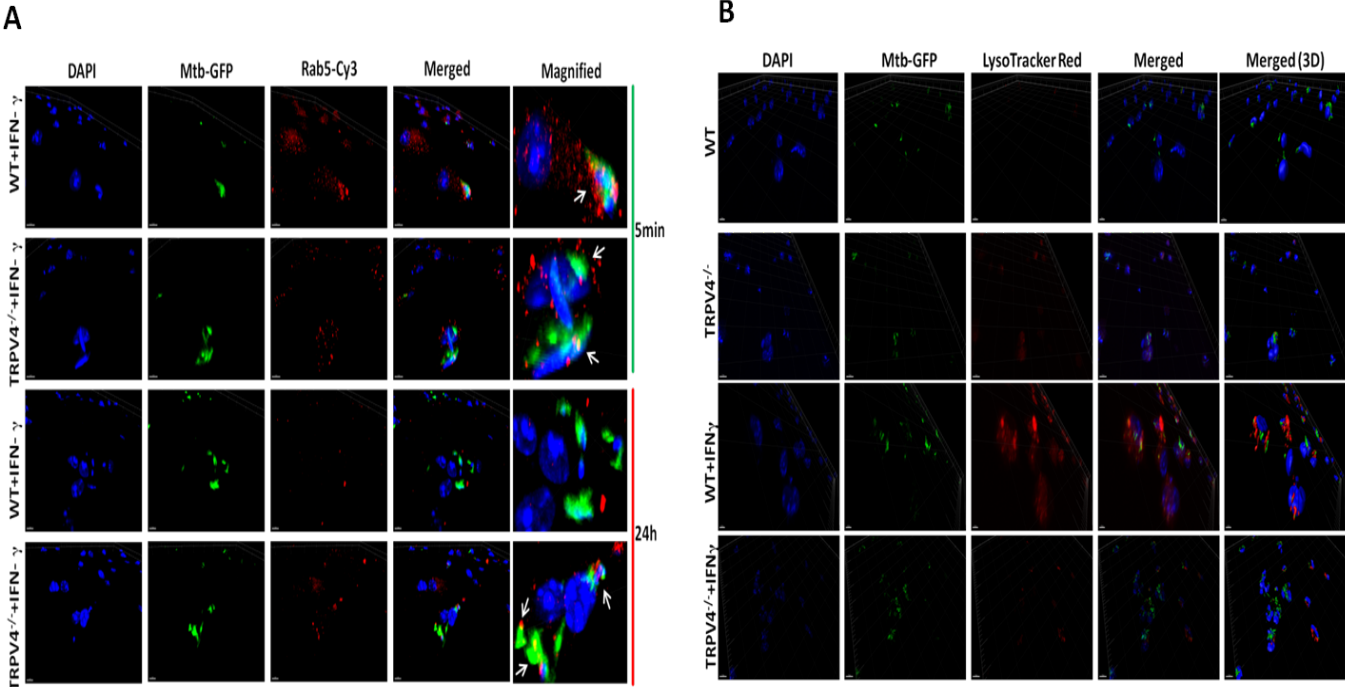
Figure S2

(A) Images showing different image channels for nuclei, *M. tuberculosis* and Rab5 as shown in Fig. 2A. **(B)** Images showing different image channels for nuclei, *M. tuberculosis* and lysotracker as shown in Fig. 2C.

Figure S3   Related to Figure 4 and Figure 5
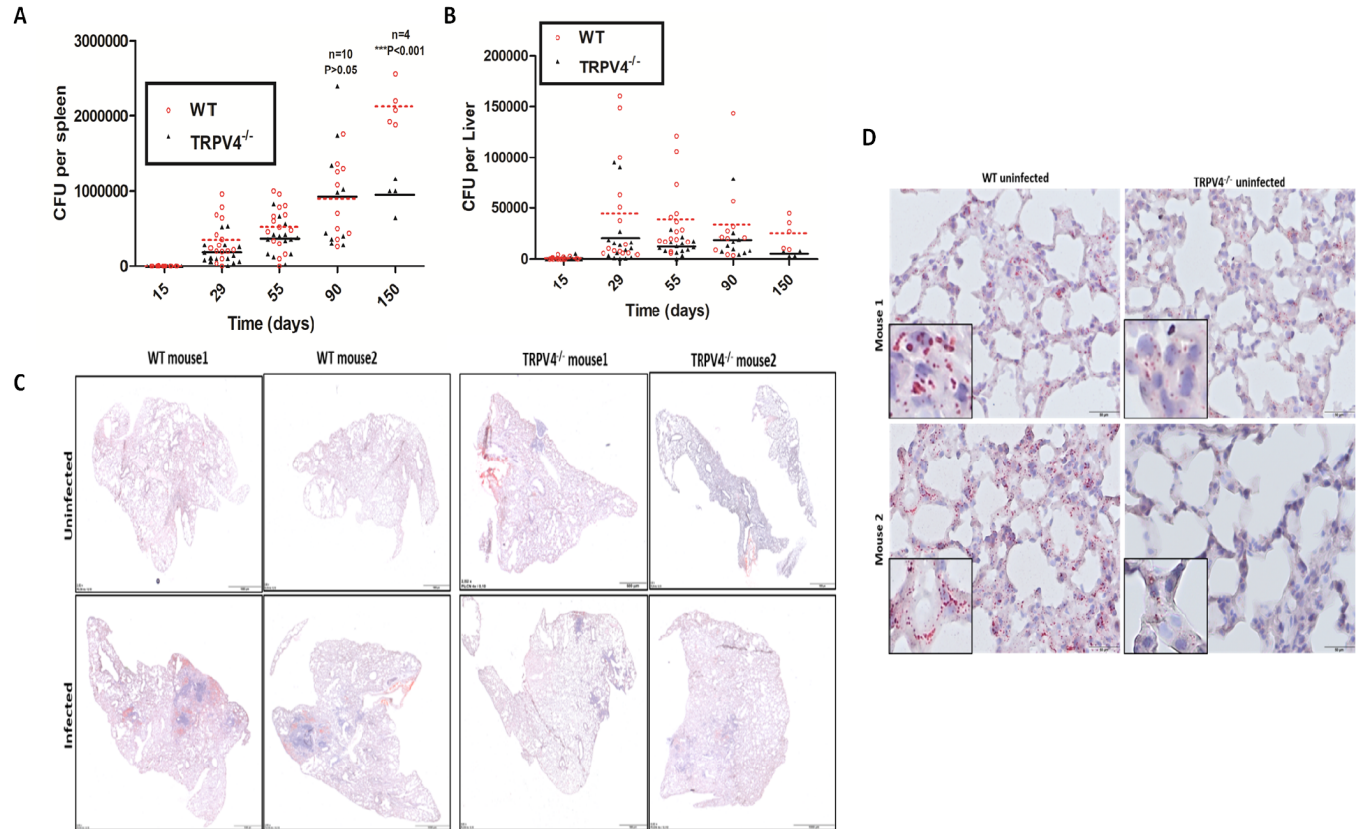
Figure S3

(A), (B) *M. tuberculosis* counts from spleen and liver of individual *M. tuberculosis* infected mice at different time points p.i. Data shown are from 3 independent experiments and each point represents one mouse. Statistical analysis was performed with Two Way ANOVA Bonferroni posttests. ***P<0.001. **(C)** Complete lung section of uninfected and *M. tuberculosis* infected mice showing oil red O stained lipid bodies (pink) at day 55 p.i. **(D)** Tissue section showing oil red O positive lipid bodies in uninfected WT and *Trpv4*$^{-/-}$ mice. Nuclei = DAPI/blue.

Figure S4   Related to Figure 5
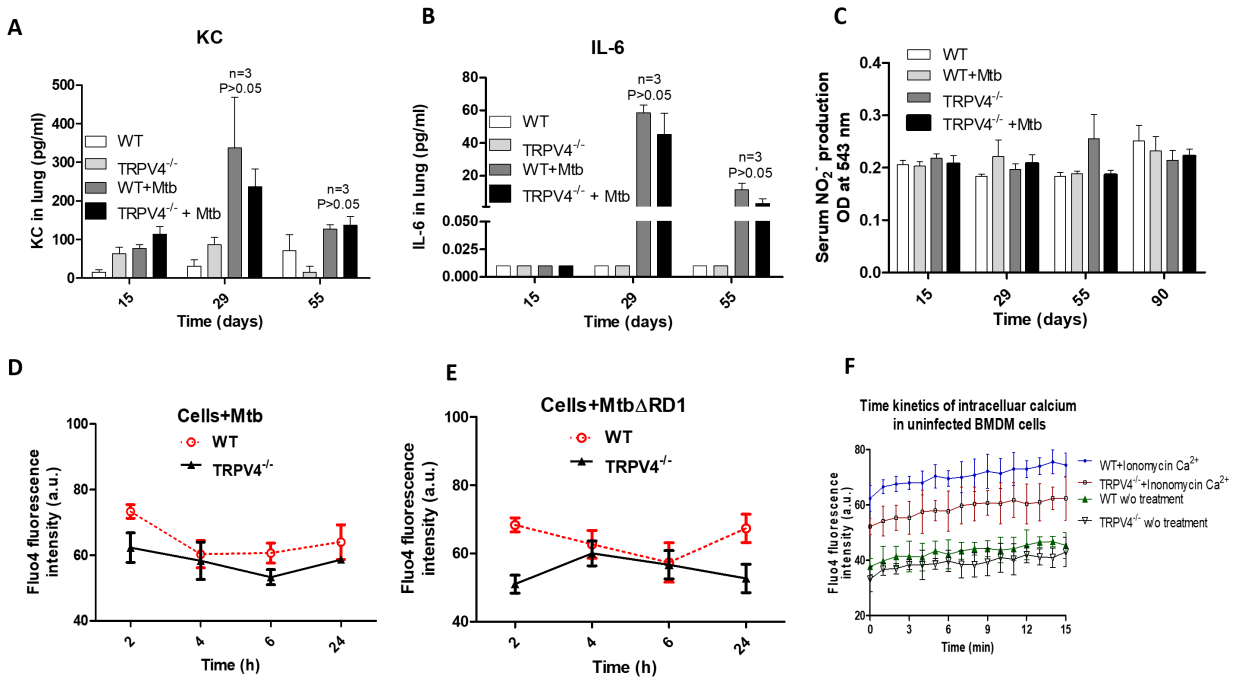
Figure S4

(A), (B) Expression of KC and IL-6 in lung lysates from WT and *Trpv4^-/-* mice at different time points p.i. **(C)** Nitrite production was measured in lung lysates prepared from *M. tuberculosis* infected WT and *Trpv4^-/-* mice at indicated time points using Nitrate reductase and Griess reagent. The NO_2^- production was represented as the absorbance of Griess reagent at 543nm. **(D,E)** Intracellular calcium levels in *M. tuberculosis* or MtbΔRD1 infected WT and *Trpv4^-/-* BMDM was measured by incubating the cells with permeable Fluo4AM (4µg/ml) dye for 30 minutes in dark. Fluorescence intensity of Fluo4AM was measured at Ex/Em of 494/506 nm using Biotek multiplate reader. **(F)** Intracellular calcium level in resting WT and TRPV4^-/-macrophages in presence of ionomycin Ca^{2+}.Statistical analysis was performed with Two Way ANOVA Bonferroni posttests.

Transparent Methods

Statement

All experiments and methods were performed in accordance with institutional guidelines and regulations. Animal studies were approved by the Ministry of Energy, Agriculture, Environment, Nature and Digitization of the state of Schleswig-Holstein, Germany [V 242-71197/2017(14-2/18)]. Experiments performed with primary human cells were reviewed and approved by the Ethics Committee of the University of Lübeck, Germany (#13-032). Study with human TB patient samples were approved by the Ethics Committee of the University of Lübeck, Germany (Ethical Approval No.14-032 and #18-194).

Bacterial strains, Cells and Reagents

M. tuberculosis H37Rv, green fluorescent protein (GFP) tagged *M. tuberculosis* (Mtb-GFP), Discosoma Red fluorescent protein (DsRed) expressing *M. tuberculosis*, Region of Difference-1 (RD1) deleted *M. tuberculosis* (MtbΔRD1), MtbΔRD1-GFP and *M. smegmatis* were cultured as described previously (Dallenga et al., 2017). To stabilize GFP and Ds-Red expression, the bacteria were grown in 7H9 media supplemented with hygromycin-B (50 µg/ml), kanamycin (20 µg/ml) and hygromycin-B (50 µg/ml), respectively. Primary antibodies directed against Trpv4 (#ACC034, Alomone lab), Rab5 (#GTX108605, GeneTex), neutrophil elastase (#51-862, proSci-ELAN)were used in this study. Secondary antibodies goat anti rabbit-cy3 (#111-165-144) were procured from Jackson Immunoresearch, UK.

Murine alveolar and peritoneal macrophages from both male and female mice were isolated from broncho-alveolar and peritoneal lavages obtained from C57BL/6J WT or *Trpv4*-knockout (*Trpv4$^{-/-}$*) mice as described previously (Schneider et al., 2014). The isolated cells were suspended

in DMEM medium containing 10 % heat inactivated fetal bovine serum (FBS) and 2 mM L-glutamine, plated (1×10^5 cells per well) on 96-well tissue culture plates and incubated in 5% CO_2 at 37^0C for at least 3 hours to allow macrophages to adhere.

Bone marrow derived macrophages (BMDM) from both male and female WT or *Trpv4^{-/-}* mice were harvested by flushing femurs and tibias as described previously (Herbst et al., 2011). Harvested cells were differentiated in DMEM containing 10% heat inactivated FBS, 2 mM L-glutamine and L929 cell supernatant (20% v/v) as a source of colony stimulating factor for one week at 37^0C and 5% CO_2.

Animal model, *M. tuberculosis* infection and CFU assay

*Trpv4^{-/-}*mice were generated on a C57BL/6J background as described previously (Liedtke and Friedman, 2003). Both WT and *Trpv4^{-/-}*mice were bred and housed under specific pathogen free (SPF) condition at the Research Center Borstel-Leibniz Lung Center (RCB). Animal studies were approved by the Ministry of Energy, Agriculture, Environment, Nature and Digitization of the state of Schleswig-Holstein, Germany [V 242-71197/2017(14-2/18)].

For aerosol infection, 6-8 weeks old both male and female mice were infected with *M. tuberculosis*-H37Rv (100 CFU) using an aerosol chamber (GlasCol, USA). After aerosol challenge, bacterial load in lung, spleen and liver was determined at different time points by mechanical disruption of organs in 0.1% v/v tween 80 in milliQ water containing a protease inhibitor cocktail (Roche Diagnostics). Ten-fold serial dilutions of organ homogenates in 0.01% v/v tween 80 and 0.05% w/v albumin were plated onto Middlebrook 7H11 agar plates and colonies were counted after 3-4 weeks of incubation at $37^0\,C$.

Macrophage infection assay

Bacterial cultures in mid-exponential phase were pelleted, washed with 1X PBS (pH 7.4). Bacterial clumps were removed by passing five times through a 27G blunt needle. *M. tuberculosis*-H37Rv culture at a final optical density of 0.1 at 600 nm (OD_{600}), which corresponds to 5×10^7 bacteria ml^{-1} was prepared with DMEM. 1×10^5 macrophages were infected at MOI 1 or otherwise as indicated. For activation of macrophages, cells were incubated overnight with 500 units/ml of IFN-γ prior to the infection. After 2 h of infection, cells were washed 3 times with 1X PBS to remove any extracellular bacteria. At different time points p.i., cells were lysed with ice cold 0.5% triton X-100, serially diluted with 1X PBS and plated on 7H11 agar plates. *M. tuberculosis* colonies were enumerated after 3 weeks of incubation at 37^0 C.

Isolation of human monocyte-derived macrophages

Human monocyte-derived macrophages (hMDM) from both male and female donors were generated from peripheral blood mononuclear cells (PBMCs) (purity consistently >92%) by elutriation and differentiated after 7 days in Teflon bag cultures in the presence of 10 ng/ml recombinant human M-CSF (VueLife 72C; Cellgenix, Freiburg, Germany) as described previously(Reiling et al., 2001). All experiments performed with primary human cells were reviewed and approved by the Ethics Committee of the University of Lübeck, Germany (#13-032).

Quantitative Real-time PCR

Total RNA was isolated from macrophages (0.2×10^6) using Trizol (peqGOLDTriFast™, USA) according to the manufacturer's instructions. cDNA was synthesized using Maxima First Strand cDNA Synthesis Kit (Thermo Fisher). Gene-specific primers and TaqMan probes (Roche Applied Science, Germany) were designed usingUniversal Probe Library (UPL) assay design center (ProbeFinder Version 2.45). qRT-PCR was performed using the LightCycler 480 Probe Master

Kit and the LightCycler 480 II system (Roche Applied Science)(Neumann et al., 2010). Crossing point values of target and reference gene were determined by the second derivative maximum method. Relative gene expression was calculated using E-Method (https://www.nature.com/app_notes/nmeth/2006/062706/full/nmeth894.html).

Human TB patient samples

All experiments performed with primary human macrophages or the staining of human lung tissues derived from patients suffering from TB, which underwent surgery for lung tissue resection as part of the anti-TB therapy, were reviewed and approved by the Ethics Committee of the University of Lübeck, Germany (Ethical Approval No.14-032 and #18-194). Lung sections were obtained from both male and female TB patients. Figure 6A,C are samples from male patient and Figure 6B and Figure 7C are samples from female TB patients.

Immunofluorescence microscopy

WT and $Trpv4^{-/-}$BMDM (1×10^5) were seeded on coverslips and infected with *M. tuberculosis* -GFP or *M. tuberculosis* ΔRD1-GFP (MOI 5) as described above. At specific time points, cells were fixed overnight with 4% PFA, washed with 1X PBS, permeabilized with 0.5 % saponin (#558255, Calbiochem) for 10 minutes and then blocked with 10 % goat serum. Cells were then incubated with primary antibodies (Rab5 -5µg/ml; TRPV4- 4µg/ml; Neutrophil elastase- 5µg/ml) for 1h at room temperature followed by washing andfluorophore-conjugated secondary antibody (Goat anti rabbit-cy3 -2.5µg/ml) in dark for 1h each step. DAPI (#D1306, Thermofisher) staining was performed at 1:1000 dilution and incubated in dark for 7 minutes. After mounting, cells were observed under fluorescence microscope (Nikon eclipse Ti) and confocal microscope (Leica TCS SP5). Confocal images were analyzed with IMARIS life-science software. Fluorescence intensities were quantified using Fiji ImageJ software.

Phagosomal pH measurement

Phagosomal pH was measured by ratiometric fluorescence microscopy (Nunes et al., 2015). To this end, *Escherichia coli* (*E. coli*) was first grown till mid-exponential phase and fixed with 4% PFA for 1 h followed by labelling with fluorescence isothiocyanate (FITC) (0.1mg/ml). WT and *Trpv4*$^{-/-}$ BMDM (1×10^5 cells) were incubated with FITC labelled *E.coli* (MOI 10) and live cell imaging was performed for 45 minutes at 37^0C and 5% CO_2 growth conditions using confocal microscopy. FITC signal was captured at excitation wavelength of 488 nm and 458 nm. Fluorescence property of FITC is quenched by acidic pH when excited at approximately 488 nm but not when excited at 458 nm. The ratio of 488/458 was used to determine the pH of the phagosome. Finally, the observed ratio value was converted into pH value by using an equation $X=17.5035\times\{-(y-10.5627)/(y-5843007)\}^{\wedge}0.0761506748$ with the help of a standard curve obtained from *E. coli*-FITC 488/458 ratio at different pH (where X=pH value and y=ratio of 488/458). In total, 15 phagosomes were analyzed from three individual biological replicates.

Lysotracker staining

BMDM (1×10^5/well) were seeded onto cover slips and infected with *M. tuberculosis*-GFP (MOI 5) for 2 h and washed. After 48 h of further incubation, cells were washed and incubated with DMEM containing the acidotropic dye, lysotracker Red (100nM; L12492, Invitrogen), for 1h in dark. Cells were fixed with 4% PFA and observed under confocal microscope with excitation/emission of 647/668nm for lysotracker red.

Cell death analysis

BMDM (1×10^5/well) were infected with WT or ΔRD1 *M. tuberculosis* and necrotic cell death was measured using Sytox green (S7020, Thermo) as per the manufacturer's instruction. Apoptotic cell

death was studied using CellEvent Caspase3/7 green detection kit (C10423, Invitrogen) as per manufacturer's instruction. Briefly, BMDM (1×10^5) were seeded on a four chambered tissue culture disc, treated with IFN-γ overnight and then infected with *M. tuberculosis*-DsRed at MOI 5. Three hours p.i., cells were washed with 1x PBS to remove extracellular bacteria followed by addition of caspase3/7 green detection reagent (10μM in DMEM media). Live cell imaging was performed till 72 h p.i. using biostation IMq imaging system (Nikon).

Determination of NO$_2^-$ production

IFN-γ activated WT and *Trpv4$^{-/-}$*BMDM (1×10^5) were infected with *M. tuberculosis*-H37Rv at MOI 5 for 24 h before supernatants were harvested and developed using Griess reagent and measured at 543nm.

For the measurement of nitrite produced under *in-vivo* conditions, lung lysates and serum were collected from *M. tuberculosis* exposed WT and *Trpv4$^{-/-}$*mice. For serum, blood was collected from inferior vena cava of mice at different time points p.i. and serum was separated using Z-gel tubes (Sarstedt; 41.1500.005) followed by centrifugation at 6000 g for 5 minutes. 40 μl of serum or lung lysate samples were incubated with 40 μl of reduction reagent (NADPH 1mg ml^{-1}; FAD 5mM; KH$_2$PO$_4$ 0.5M, pH 7.5 with 0.25U of nitrate reductase-N7265-Sigma) at 37^{0}C for 2 h (Petricevich et al., 2000). After incubation, 80 μl of Griess reagent was added and incubated for 15 minutes in dark. OD was measured at 543nm.

Western blot analysis

Macrophage cells (1×10^6) were infected with WT and ΔRD1 *M. tuberculosis* at MOI 5. Then cells were harvested, lysed in RIPA buffer and electrophoresed to SDS-PAGE and western blotting as described previously(Mohanty et al., 2016). Membranes were then incubated overnight with the

primary anti-Trpv4 antibody (Alomone lab; ACC-034), washed, further incubated with HRP conjugated secondary antibody for 2 h at RT and developed and imaged using chemiluminescence and the ChemiDoc Imaging system (Bio-Rad), respectively.

Immunohistochemistry and Histopathology

Lungs from *M. tuberculosis* infected WT and *Trpv4$^{-/-}$* mice were harvested at different time points, incubated with 4% PFA overnight for fixation and 4 µm tissue sections were prepared. For cryo-sections, PFA fixed tissues were incubated with 1X PBS overnight at 4^{0}C, transferred to increasing concentrations of saccharose (5-20%) and embedded in 20% saccharose/ tissuetek (2:1). 4 µm cryo-sections were prepared with Leica cryostat at -20^{0}C.

Paraffin sections were used for immunohistochemistry by deparaffination of tissue sections and antigen retrieval in citrate buffer (pH 6.0). Endogenous peroxidase was inhibited with H$_2$O$_2$ and blocking was done with 10% serum followed by overnight incubation with primary antibody at 4 ^{0}C. Tissue sections were washed 3 times in 1X PBS followed by incubation with biotin conjugated secondary antibody (2.6 µg/ml or 1:500 goat-anti rabbit #111066047, Jackson Labs) for 45 minutes at RT and avidin-biotin complex for 45 minutes at RT (Vectastain Elite ABC-Peroxidase Kit, #VC-PK-6100-KI01). Tissue sections were developed in DAB followed by nuclei staining with hematoxyline. Similar staining procedure was used for immunohistochemistry analysis of human patient suffering from TB lung tissues. For *M. tuberculosis* counts, tissue sections were stained with Ziehl-Neelsen followed by nuclei staining with hematoxylin. Slides were embedded in Entellan.

For lipid staining, lung cryo-sections were washed 3 times with 1X PBS followed by incubation with Oil Red O stain for 30 minutes at room temperature. After incubation, slides were washed 3 times with 1X PBS and the nuclei were counterstained in hematoxylin. Slides were

embedded in Kaiser's Glycerin Gelatine and observed by light microscopy (Olympus BX41). Images were captured with CellSens standard Olympus software.

Cytokine and chemokine analysis

Cytokines and chemokines in mouse lung lysate and serum were analyzed using U-plex MSD kits (#K15069L) and the assay was performed according to the manufacturer's instructions.

Intracellular calcium measurement

BMDM ($1x10^5$ cells per well) from WT and $Trpv4^{-/-}$ mouse were seeded in a 96 well plate. Cells were treated with 4μM Ionomycin, 2mM $CaCl_2$ or infected with *M. tuberculosis*-H37Rv or *M. tuberculosis*ΔRD1 with a MOI 5. At indicated time points, media were removed and cells were washed twice with 1xPBS. Cells were then incubated with Fluo-4AM (4μg/ml) for 30 minutes at 37 ^{0}C in dark, and the fluorescence intensity was obtained at Ex/Em of 494/506 nm using Biotek multiplate reader.

Statistical analysis

Data are presented as mean ± standard error mean (SEM). Two-way and One-way analysis of variance was used to determine statistical significance between groups where $*p < 0.05$, $**p < 0.01$, $***p < 0.001$. All statistical significances between the experimental groups are marked.

KEY RESOURCES TABLE

REAGENT or RESOURCE	SOURCE	IDENTIFIER
Antibodies		
TRPV4	Alomone lab	ACC034
Rab5	GeneTex	GTX108605
Neutrophil elastase	proSci-ELAN	51-862
Goat anti rabbit-cy3	Jackson immunoresearch	111-165-144
Goat-anti rabbit biotin conjugated	Jackson immunoresearch	111-066-047
Goat-anti rabbit HRP conjugated	Jackson immunoresearch	111-035-045
Bacterial and Virus Strains		
M. tuberculosis H37Rv	Schaible lab, Research Center Borstel, Germany	N/A
M. tuberculosis H37Rv GFP	Tanya Parish, Center for Global Infectious Disease Research Seattle	N/A
M. tuberculosis H37Rv ΔRD1	Suzanne M. Hingley-Wilson, William R. Jacobs	N/A
M. tuberculosis H37Rv DsRed	Schaible lab, Research Center Borstel, Germany	N/A
M. smegmatis mc^{2}155	Schaible lab, Research Center Borstel, Germany	N/A
E. coli	Schaible lab, Research Center Borstel, Germany	N/A
Biological Samples / Cell line		
Human TB patient lung sample	Luebeck University, Germany	Ethical Approval No.14-032 and #18-194
RAW264.7 mouse macrophages	A. Sonawane lab, India	N/A
Chemicals, Peptides, and Recombinant Proteins		
7H11 agar media	Difco	283810
DMEM	Pan Biotech	P04-03600
RPMI	Pan Biotech	P04-17500

Kanamycin	Roth	T832.1
Hygromycin-B	Pan Biotech	P06-08020
FBS	Pan Biotech	P30-3306
L-glutamine	Pan Biotech	P04-80100
Tween-80	Roth	4780
Protease inhibitor cocktail	Roche	4693132001
DAPI	Thermofisher	D1306
TritonX-100	Roth	3051.3
Trizol Tri Reagent	Zymo Research	R2050-1-200
Lysotracker red	Invitrogen	L12492
Caspase 3/7 detection kit	Invitrogen	C10423
FITC	Sigma	F7250
RN1734	Sigma	R0658
Recombinant murine IFN-γ	Peprotech	315-05
Flou4AM	Goswami lab, NISER, India	N/A
Ionomycin	Goswami lab, NISER, India	N/A
TB Carbolfuchsin	BD	212518
Mayer's Haematoxylin	Roth	T865.2
Eosin	Roth	7089.2
Entellan	VWR	1079610500
Sucrose	Roth	9286.1
Tissue tek	Leica	020108926
Methylbutane	VWR	720-0821
Oil Red O	Sigma	O0625
Nitrate reductase	Sigma	N7265
NADPH	Sigma	N7265-2UN
FAD	Sigma	F6625-10MG
KH_2PO_4	Merck	1.04873.0250
DAB for immunohistochemistry	Sigma	D4293-50SET
Avidin Biotin Complex kit	Vector lab	VC-PK-6100-KI01

Critical Commercial Assays		
MSD kit for cytokine analysis	Meso Scale Discovery	K15069L
Experimental Models: Organisms/Strains		
TRPV4$^{-/-}$ mouse	Liedtke *et al.* 2003	N/A
Oligonucleotides		
Human TRPV4 forward primer for mRNA expression CTCTTCATGATCGGCTACGC	Roche	Probe-54
Human TRPV4 reverse primer for mRNA expression ACACCTTCATGTTGGCACAC	Roche	Probe-54
Human HPRT forward primer for mRNA expression TGACCTTGATTTATTTTGCATACC	Roche	Probe-73
Human HPRT reverse primer for mRNA expression CGAGCAAGACGTTCAGTCCT	Roche	Probe-73
Software and Algorithms		
Imaris 7	Bitplane	http://www.bitplane.com/imaris/imaris
GraphPad Prism	GraphPad	https://www.graphpad.com/scientific-software/prism/
Graphical abstract	BioRender	Created with BioRender.com

Supplemental References

Dallenga, T., Repnik, U., Corleis, B., Eich, J., Reimer, R., Griffiths, G.W., and Schaible, U.E. (2017). M. tuberculosis-Induced Necrosis of Infected Neutrophils Promotes Bacterial Growth Following Phagocytosis by Macrophages. Cell Host Microbe *22*, 519-530.e513.

Herbst, S., Schaible, U.E., and Schneider, B.E. (2011). Interferon gamma activated macrophages kill mycobacteria by nitric oxide induced apoptosis. PloS one *6*, e19105.

Liedtke, W., and Friedman, J.M. (2003). Abnormal osmotic regulation in trpv4-/- mice. Proceedings of the National Academy of Sciences of the United States of America *100*, 13698-13703.

Mohanty, S., Dal Molin, M., Ganguli, G., Padhi, A., Jena, P., Selchow, P., Sengupta, S., Meuli, M., Sander, P., and Sonawane, A. (2016). Mycobacterium tuberculosis EsxO (Rv2346c) promotes bacillary survival by inducing oxidative stress mediated genomic instability in macrophages. Tuberculosis (Edinb) *96*, 44-57.

Neumann, J., Schaale, K., Farhat, K., Endermann, T., Ulmer, A.J., Ehlers, S., and Reiling, N. (2010). Frizzled1 is a marker of inflammatory macrophages, and its ligand Wnt3a is involved in reprogramming Mycobacterium tuberculosis-infected macrophages. Faseb j *24*, 4599-4612.

Nunes, P., Guido, D., and Demaurex, N. (2015). Measuring Phagosome pH by Ratiometric Fluorescence Microscopy. Journal of visualized experiments : JoVE, e53402.

Petricevich, V.L., Teixeira, C.F., Tambourgi, D.V., and Gutierrez, J.M. (2000). Increments in serum cytokine and nitric oxide levels in mice injected with Bothrops asper and Bothrops jararaca snake venoms. Toxicon : official journal of the International Society on Toxinology *38*, 1253-1266.

Reiling, N., Blumenthal, A., Flad, H.D., Ernst, M., and Ehlers, S. (2001). Mycobacteria-induced TNF-alpha and IL-10 formation by human macrophages is differentially regulated at the level of mitogen-activated protein kinase activity. J Immunol *167*, 3339-3345.

Schneider, B.E., Behrends, J., Hagens, K., Harmel, N., Shayman, J.A., and Schaible, U.E. (2014). Lysosomal phospholipase A2: a novel player in host immunity to Mycobacterium tuberculosis. European journal of immunology *44*, 2394-2404.